NON-REACTING CFD ANALYSIS OF A DROP TUBE FURNACE USED FOR SOLID FUEL COMBUSTION

A THESIS SUBMITTED TO
THE GRADUATE SCHOOL OF NATURAL AND APPLIED SCIENCES
OF
MIDDLE EAST TECHNICAL UNIVERSITY

BY

GAMZE GÜLENÇ

IN PARTIAL FULFILLMENT OF THE REQUIREMENTS
FOR
THE DEGREE OF MASTER OF SCIENCE
IN
MECHANICAL ENGINEERING

OCTOBER 2017

Approval of the thesis:

NON-REACTING CFD ANALYSIS OF A DROP TUBE FURNACE USED FOR SOLID FUEL COMBUSTION

submitted by **GAMZE GÜLENÇ** in partial fulfillment of the requirements for the degree of **Master of Science in Mechanical Engineering Department, Middle East Technical University** by,

Prof. Dr. Gülbin Dural Ünver _____
Dean, Graduate School of **Natural and Applied Sciences**

Prof. Dr. M.A. Sahir Arıkan _____
Head of Department, **Mechanical Engineering**

Asst. Prof. Dr. Feyza Kazanç _____
Supervisor, **Mechanical Engineering Dept., METU**

Examining Committee Members:

Assoc. Prof. Dr. Cüneyt Sert _____
Mechanical Engineering Dept., METU

Asst. Prof. Dr. Feyza Kazanç _____
Mechanical Engineering Dept., METU

Assoc. Prof. Dr. M. Metin Yavuz _____
Mechanical Engineering Dept., METU

Asst. Prof. Dr. F. Nazlı Dönmezer Akgün _____
Mechanical Engineering Dept., Boğaziçi University

Asst. Prof. Dr. Sıtkı Uslu _____
Mechanical Engineering Dept., TOBB ETU

Date: 04.10.2017

I hereby declare that all information in this document has been obtained and presented in accordance with academic rules and ethical conduct. I also declare that, as required by these rules and conduct, I have fully cited and referenced all material and results that are not original to this work.

Name, Last name : Gamze GÜLENÇ

Signature :

ABSTRACT

NON-REACTING CFD ANALYSIS OF A DROP TUBE FURNACE USED FOR SOLID FUEL COMBUSTION

Gülenç, Gamze

M.S., Department of Mechanical Engineering

Supervisor: Asst. Prof. Dr. Feyza Kazanç

October 2017, pages 77

In this thesis, the flow inside the drop tube furnace (DTF) which was already built in the Clean Combustion Technologies Laboratory located in Department of Mechanical Engineering at Middle East Technical University is analysed by using Computational Fluid Dynamics method. DTF is a semi-pilot scale electrically heated reactor with the aim of achieving constant temperature zone to investigate combustion characteristics of solid fuels. A simplified geometry is created for the flow analysis inside the DTF. The heating zone of the reactor is heated up to 1273 K and total air volumetric rate entering the inlets of the furnace is 10 L/min for the analyses conducted in the thesis. Natural convection governs the flow inside the furnace. Three different turbulence models (Standard k-ε, Realizable k-ε and SST k-ω) are employed in order to obtain velocity magnitudes and temperature distribution in the DTF. Transient solution is used for the simulation in which SST k-ω model is utilized to achieve convergence. The results are compared to analysis results in literature and temperature measurements performed. The analyses using k-ε models provide more similar trends with analysis results in literature and measurements. Constant temperature zone is achieved with k-ε models. Furthermore, gravitational

effect is investigated. In the analysis where gravitational effect is neglected, the air continues to flow through the whole reactor with the declining velocity from 0.3 m/s to 0.1 m/s. However, in reality, the flow is stagnant at the exit of the heating zone, and the flow is maintained using a vacuum pump.

Keywords: Drop Tube Furnace, Computational Fluid Dynamics (CFD), Natural Convection, Combustion

ÖZ

KATI YAKIT YANMASI İÇİN KULLANILAN DÜŞEY BORULU FIRININ TEPKİME OLMADAN HESAPLAMALI AKIŞKANLAR DİNAMİĞİ YÖNTEMİYLE ANALİZİ

Gülenç, Gamze

Yüksek Lisans, Makina Mühendisliği Bölümü

Tez Yöneticisi: Yrd. Doç.Dr. Feyza Kazanç

Ekim 2017, sayfa 77

Bu tezde, Orta Doğu Teknik Üniversitesi Makina Mühendisliği bölümü Temiz Yanma Teknolojileri Laboratuvarında bulunan bir düşey borulu fırın Hesaplamalı Akışkanlar Dinamiği yöntemi kullanılarak analiz edilmiştir. Düşey borulu fırın, katı yakıtların yanma karakteristiklerini soruşturmak için sabit sıcaklık bölgesi elde etmek amacıyla elektrikle ısıtılan reaktördür. Fırın içindeki akışı analiz etmek için düşey borulu fırının basitleştirilmiş geometrisi yaratılmıştır. Bu tezde yapılan analizler için, reaktörün ısıtılan bölgesi 1273 K ‘e ısıtılmıştır ve fırının inletlerine giriş yapan toplam hava oranı 10 L/dak ‘dır. Hız büyüklüklerini ve sıcaklık dağılımlarını elde etmek için üç farklı türbülanslı model (Standard k-ε, Realizable k-ε and SST k-ω) kullanılmıştır. Zamana bağlı çözüm, SST k-ω ile yapılan analizde yakınsama elde etmek için kullanılmıştır. Sonuçlar, literatürdeki analiz sonuçları ve yapılan sıcaklık ölçümleri ile karşılaştırılmıştır. k-ε model kullanılan analizler literatür sonuçlarıyla ve ölçümlerle daha benzer trendler sağlamıştır. k-ε modellerle sabit sıcaklık bölgesi sağlanmıştır. Ayrıca, yerçekimsel etki soruşturulmuştur. Yerçekiminin ihmal edildiği analizde, hava bütün reaktör boyunca 0,3 m/s’den 0,1

m/s’ye azalan bir hızla akmaya devam etmiştir. Fakat gerçekte, akış ısıtılan bölgenin çıkışında durgundur ve bir vakum pompası kullanılarak sürdürülmektedir.

Anahtar Kelimeler: Düşey borulu fırın, Hesaplamalı Akışkanlar Dinamiği, Doğal Taşınım, Yanma

To My Family,

ACKNOWLEDGEMENTS

I would like to thank my supervisor Asst. Prof. Dr. Feyza Kazanç for her guidance and advice throughout this thesis.

I would like to thank the examining committee members for their comments on my thesis.

I would like to thank the members of Clean Combustion Technologies Laboratory for the productive study environment. Particularly, I would like to thank Duarte Magalhães for the experimental results and his helps.

I would like to thank my mother, father and sister for their supports, motivation and understandings during this thesis.

This research was supported by the METU-BAP (Grant no: BAP-08-11-2015-022).

TABLE OF CONTENTS

LIST OF TABLES

TABLES

LIST OF FIGURES

FIGURES

NOMENCLATURE

A: Surface Area (m^2)

CFD: Computational Fluid Dynamics

C_p: Specific Heat Capacity (J/kg.K)

d: Diameter (mm)

DTF: Drop Tube Furnace

g: Gravity (m/s^2)

Gr: Grashof Number

h: Heat Transfer Coefficient ($W/m^2.K$)

I: Turbulence intensity

k: Turbulence kinetic energy (m^2/s^2)

k_c: Thermal Conductivity (kW/m.K)

Nu: Nusselt Number

Pr: Prandtl Number

Ra: Rayleigh Number

Re: Reynolds Number

SST: Shear Stress Transport

T_g: True Gas Temperature

T_{TC}: Thermocouple Temperature

V: Velocity (m/s)

ε: Rate of dissipation of turbulence (m^2/s^3)

ω: Rate of specific dissipation of turbulence (s^{-1})

$\dot{V}$: Volume flow rate (m^3/s)

ϵ: Surface Emissivity

σ: Stephan-Boltzmann Constant ($W/m^2.K^4$)

ρ: Density (kg/m^3)

β: Volume Expansion Coefficient (1/K)

μ: Dynamic Viscosity (kg/m.s)

ν: Kinematic Viscosity (m^2/s)

CHAPTER 1

INTRODUCTION

1.1 Energy Production from Coal and Biomass

The global energy consumption has been increasing in the last decades due to increased industrialization, food production, transport, and growth in population [1]. Global total primary energy supply from 1971 to 2015 is demonstrated in Figure 1.1 [2]. Combustion is one of the main forms of energy usage [3]. Combustion of fossil fuels accounts for 81 % of the world's energy usage in 2015, as can be seen in Figure 1.2 [2, 4]. Fossil fuels can be classified into three main categories based on their phases, which are; solid, liquid, and gas. Coal can be named as the main component of the solid fossil fuel category [5].

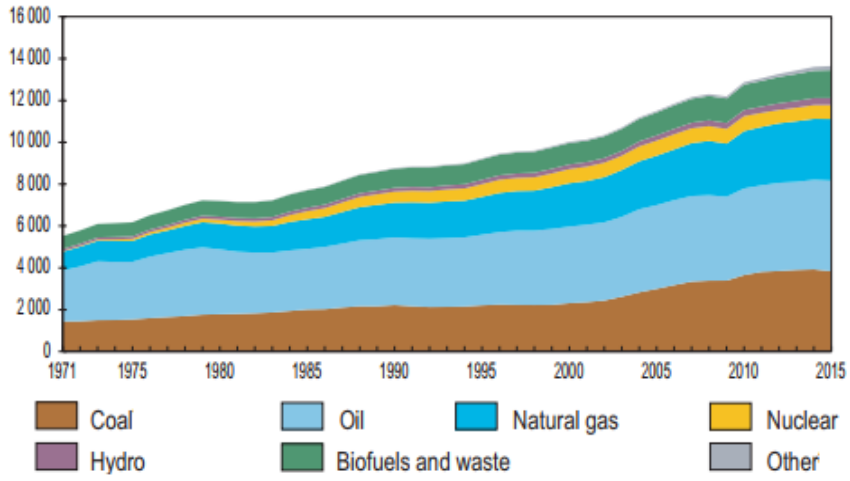

Figure 1.1 Global Total Primary Energy Supply from 1971 to 2015 by Fuel (Mtoe) [2]

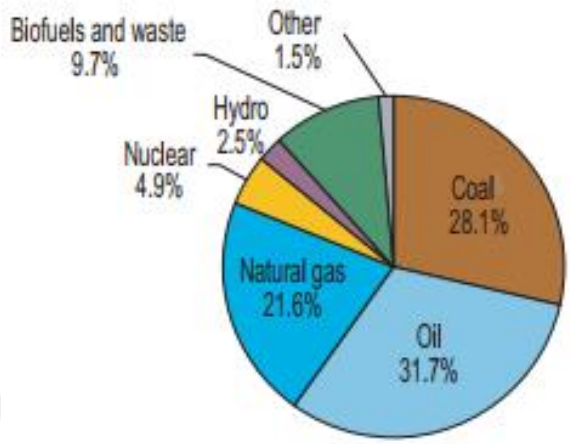

Figure 1.2 Utilization Rates of Fuels [2]

Coal: The resources and reserves of coal are the most abundant combustible energy resources on the planet [6]. Coal is a fossil fuel altered from the remains of prehistoric vegetation. Types of coal are presented in Figure 1.3. Lignite is the youngest coal among other types of coal. Lignite transforms into sub-bituminous coal with effects of temperature and pressure on lignite ongoing during many millions of years. This transformation continues until the coal becomes harder and blacker, eventually forming bituminous or hard coal [7].

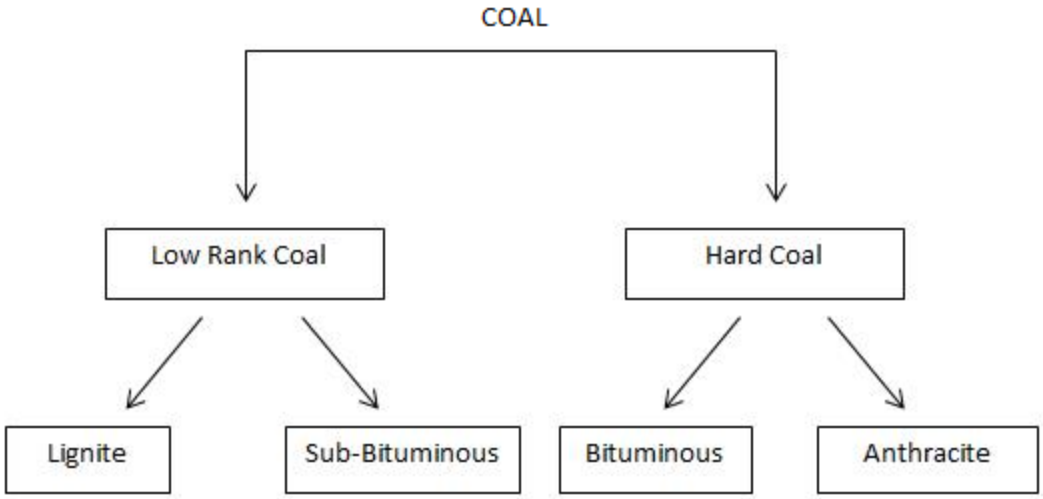

Figure 1.3 Types of Coal [7]

Coal combustion has been a significant energy resource for human being during history. Due to the fact that coal has large reserves and low cost, direct coal combustion is mostly employed for industrial and domestic purposes. On the other hand, coal has harmful effects on the environment. Coal combustion brings out pollutants, such as particulate matter, sulphur dioxide, nitrogen oxide, carbon dioxide, heavy metals, and volatile organic compounds. These pollutants have serious effects on human health. Therefore, hazardous pollutants emitted to the environment should be reduced in order to improve life quality. In order to achieve this, clean coal combustion technologies need to be developed. [8]. Coal is a major contributor to the greenhouse gases in the atmosphere, with high carbon dioxide emissions resulting from combustion; and significant methane emissions resulting from mining activities. Greenhouse gases cause global warming [9].

Coal combustion process contains four main stages as described below;

1) Moisture release
2) Devolatilization
3) Volatile combustion
4) Char combustion

In moisture release stage, moisture in the coal evaporates with an increase in coal temperature. In devolatilization stage, volatile matter is released with the heating of coal. Gases and high molecular weight compounds in coal are emitted with increasing temperature. Products of coal devolatilization include tar, hydrogen, carbon monoxide and hydrocarbon gases. Volatile matter combustion and char combustion take place after devolatilization process. Volatile matter combustion consists of homogeneous reactions, whereas char combustion is made up of heterogeneous reactions on the char surface [8]. Single coal particle combustion process can be seen in Figure 1.4.

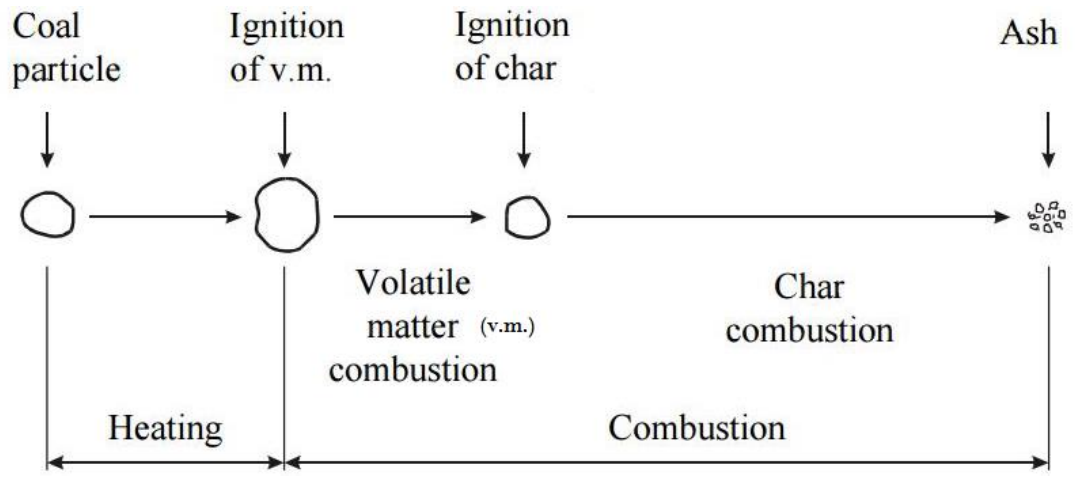

Figure 1.4 Single Coal Particle Combustion Process [10]

Biomass: Biomass is one of the renewable energy sources. These fuels are derived from living or, recently living organisms. Biomass is carbon neutral fuels as biomass fuels consume CO_2 to produce their own food during their lives, and release the approximately same amount of CO_2 when they are burned to produce energy. Biomass can be classified into four main categories: woody biomass, herbaceous biomass, fruit biomass, and blends [11]. Combustion stages of biomass are nearly same as coal combustion process, as be shown in Figure 1.5 [4].

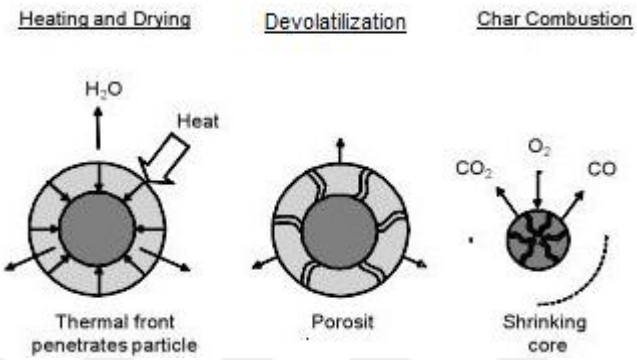

Figure 1.5 Three Main Stages for Combustion Process [4]

In drying process, fuels are heated, because all biomass consists of moisture, and this moisture has to be driven off for initiation of combustion, i.e. ignition. Radiation from flames and the stored heat in the combustion system provides the required heat for drying. As the temperature of the dry biomass is between 200 °C and 350 °C, the volatile gases are released. In oxidation process, first the released volatiles are consumed and char oxidizes at about 800 °C [4].

Biomass combustion is advantageous in terms of lower emission rates (CO_2, SO_x and NO_x) when compared with coal combustion [12]. However, energy production from biomass fuels has several shortcomings. First of all, biomass has lower energy density. Moreover, grinding and milling coal is easier than grinding and milling biomass fuels. Furthermore, there are important differences in both physical and chemical properties such as the kinetics of devolatilization, ignition and char burnout [13-14].

1.2 Coal Combustion Technologies

Coal-fired thermal power plants are one of the most conventional and reliable means of electricity generation. The chemical energy of the coal is converted into electrical energy in coal-fired thermal power plants. Boilers are used to convert chemical energy of the fuel into heat energy which is used to produce the steam. After that, steam is expanded through the turbine coupled with the generators which convert mechanical energy into electrical energy.

Power generation with coal-fired boilers accounts for 38 % of the worldwide electrical power generation [15]. Pulverized coal fired boilers are the most popular boilers, because of their high combustion efficiency and coal type flexibility. The pulverized coal and air mixture is burnt in the radiation zone (furnace) in the boiler. There are some advantages of feeding pulverized coal to the furnace. Firstly, finer particles burn faster that provides complete combustion. Also, when the coal is pulverized, soot and CO emissions in the flue gas is reduced [16]. In thermal power plants that use pulverized fuel system, primary air carries the coal to the boiler and secondary air supplements the necessary amount of air for complete combustion. A pulverized coal fired boiler is demonstrated in Figure 1.6.

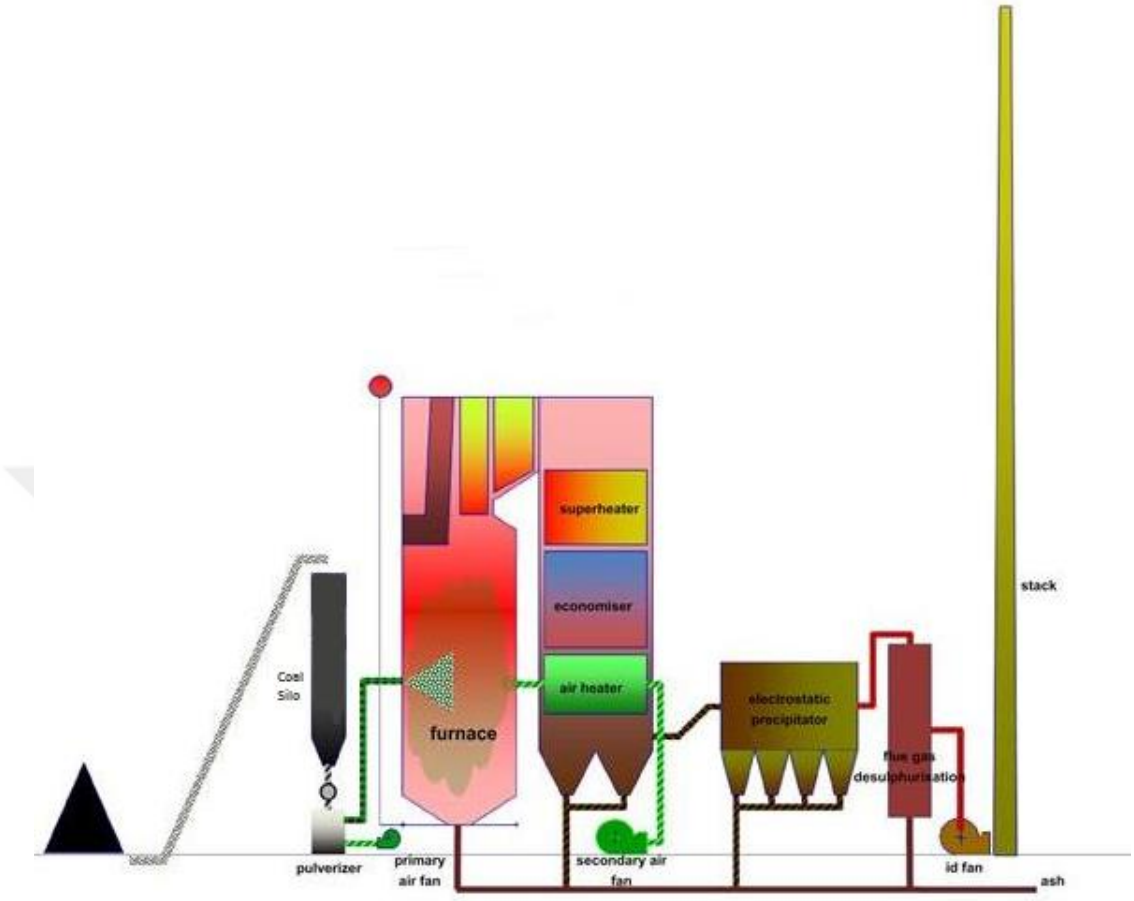

Figure 1.6 A Pulverized Coal Fired Boiler [17]

In order to comprehend the pulverized coal combustion inside the boilers and to design efficient burners, experimental studies have been conducted in literature. One of the experimental rig to study pulverized coal combustion behaviour is Drop Tube Furnace (DTF). DTF is a laboratory scale facility, which is used to simulate full-scale pulverized combustion furnaces. In DTF, certain important operating parameters encountered in large-scale boilers can be achieved, such as high temperatures and high heating rates [18].

In drop tube furnaces, pulverized fuel particles are inserted into an electrically preheated vertical reactor. Particles are inserted through a cooled injector with the help of a feeder. A vibration motor in the feeding unit provides the required vibration for pulverizing the coals. The furnace is electrically heated in order to obtain high temperature isothermal conditions which take place in large scale boilers. Reactions occur in the constant temperature zone (reaction zone). Burned particles are collected with the collection probe for sampling purposes. The experiments performed in drop tube furnaces in literature will be introduced in detail in Chapter 2, Section 2.1.

Ease of operation and achieving conditions similar to large scale combustion boilers are two main advantages of using drop tube furnace rig to simulate actual pulverized coal combustion. In DTF, high heating rates (10^5 ºC/s), high temperatures (1300ºC), and low residence time (in the order of few seconds) are achieved. Moreover, heating elements in DTF create a radiation zone which resembles the radiative zone of large scale boilers.

On the other hand, there are some shortcomings of DTF utilization. One of the disadvantages of drop tube furnace is the lack of high turbulence, which is the dominant flow regime in large scale boilers. The turbulence cannot be reproduced in drop tube furnaces. As a consequence, the interaction between the pulverized fuel particles during combustion is limited in DTF.

Combustion kinetics, residence time, temperature profile, and burnout time are important parameters for fuel combustion characterization. A drop tube furnace was built in Clean Combustion Technologies Laboratory located in Department of Mechanical Engineering at Middle East Technical University in order to obtain these parameters to characterize various coals and biomass fuels for their combustion behaviour. Detailed information regarding this drop tube furnace is presented in Chapter 3.

1.3 Motivation of the Study

Drop Tube Furnace experimental rig is used to research combustion characteristics of solid fuels as it reflects realistic pulverized combustion systems conditions. The important parameters for fuel characterization, such as combustion kinetic data, particle burnout, residence time and temperature profile can be achieved by using drop tube furnace experimental rig. A DTF (see Chapter 3 for the detailed information) was built in the Clean Combustion Technologies Laboratory located in Department of Mechanical Engineering at Middle East Technical University within the scope of TÜBİTAK Career Award, 214M332. In this TÜBİTAK project, it is aimed to investigate the pulverized combustion behaviours of co-firing various Turkish lignite coals, obtained from different locations with different chemical and physical properties, with a variety of biomasses (olive residue, grape residue, and almond shells) by using a DTF.

At this point, to know the flow in the DTF is important in order to understand the characterization of the solid fuel combustion. The main reason to study flow inside the reactor is to obtain velocity and temperature distribution along the vertical furnace. Velocity profiles are critical to provide data on the particle residence time. Temperature distribution information is vital in order to understand whether an isothermal heating zone is obtained as in the case of real furnace radiation zone. Velocity magnitude information along with temperature information is used to understand the dominating flow regime without combustion, which is helpful to isolate any disturbances that combustion may create. Velocity magnitude information is also used to achieve isokinetic sampling throughout the furnace. In order to sample particles from different vertical position of the furnace, velocity of the flow that enters the collection probe should be equal to the velocity of the suction created by a vacuum pump for the isokinetic sampling. In order to adjust the vacuum pump capacity for the isokinetic sampling at any vertical location, knowledge of the velocity magnitude is vital.

Computational Fluid Dynamics models have some advantages, which include having comprehensive information inside the system, being fast, and relatively low cost. Therefore, in this study, CFD models are used to characterize the flow inside the drop tube furnace, which is utilized for the experiments conducted within the scope of TÜBİTAK project.

1.4 Aim of the Study

In this thesis, the drop tube furnace used for solid fuel combustion experiments in Clean Combustion Technologies Laboratory is analysed with Computational Fluid Dynamics method. ANSYS FLUENT is employed as a solver.

The aim of this thesis is;

- to determine the dominant phenomena leading to a flow motion in the drop tube furnace with non-dimensional parameters,
- to get more information on the flow in the drop tube furnace, particularly in terms of temperature and velocity, through CFD simulations,
- to validate the results of CFD simulations with the experimental temperature measurements,
- to investigate gravitational effect on the flow in the DTF.

CHAPTER 2

LITERATURE REVIEW

There are several studies which are related to drop tube furnaces in literature. Studies are mainly categorized as experimental and numerical. In this chapter, firstly, drop tube furnace experiments are introduced. Secondly, numerical studies are outlined.

2.1 Drop Tube Furnace Experiments

The experiments for the examination of combustion characteristics of coals and biomass fuels have been performed in drop tube furnaces. Burnout, ignition and devolatilization processes of fuels are evaluated in these studies. Also, data for gas temperature, gas velocity and gas release along the reactor for fuels are obtained in references.

2.1.1 Combustion Characteristics of Coals

Coal is currently the main source of primary energy for the world [1]. Imported coals have been used for power generation all over the world. Therefore, an examination of the behaviour of coals is very important [19]. Cloke et al. [19] investigated the combustion behaviours of fourteen coals by using a DTF. Card and Jones [20] studied the combustion of pulverized coal in a DTF with optical techniques. Avila et al. [21] evaluated coal char combustion in O_2/N_2 and O_2/CO_2 conditions in a drop tube furnace. The effect of oxygen concentration was observed with this study. According to this study, particle surface temperature increases with an increase in O_2 concentration. Also, particle size decreases as O_2 concentration increases. This study stated that particles travel along the centreline in the laminar flow.

Coal combustion accounts for the largest share of CO_2 emissions [22]. Oxy-fuel combustion is a technology promised for CO_2 capture from power plants. Therefore, it has gained lots of concerns. There are several studies on oxy-fuel combustion technology [23]. Wang et al. [22] investigated oxy-fuel characteristics of pulverized coal in a DTF. Rokni and Levendis [24] researched the effect of the utilization of a high-alkali coal ash for the capture of SO_2 emissions from combustion of a high-sulfur bituminous coal with the experiments in the drop tube furnace. In this research, substantial reduction in SO_2 emissions of the bituminous coal was observed with addition of lignite ashes. Zellagui et al. [25] studied particulate matter emissions during combustion of five types of coals and woody biomass in a DTF.

The ignition behaviour for fuel particles is one of the most important combustion characteristics, because it has effects on flame stability, formation and emission of pollutants and flame extinction. It is vital for the design of furnace [26-27]. Chi et al. [26] studied the ignition behaviours of pulverized coals and coal blends in a DTF with flame monitoring techniques. Cai et al. [27] researched effect of steam on ignition of pulverized bituminous coal particles in oxy-fuel combustion in a drop tube furnace. Bituminous coal is used as fuel in this work. The experiments are conducted in a DTF. The ignition processes in this drop tube furnace are recorded by using high speed camera.

2.1.2 Combustion Characteristics of Biomass Fuels

Biomass fuel is one of the most important alternative fuels to coal in energy production. However, biomass fuels have some drawbacks, such as its hydrophilic nature, low heating value, and high specific energy required in grinding. Improving these properties for biomass fuels is necessary [28]. Torrefaction is a technology which provides to improve the properties of biomass fuels. It is a pre-treatment process for biomass [13-14]. Tolvanen et al. [13] studied fine grinding and combustion behaviours of biomass fuels. These fuels are raw, torrefied, and steam-exploded wood. The experiments are conducted in a laminar drop tube furnace. McNamee et al. [14] examined combustion behaviours of high-heating rate chars from untreated and torrefied biomass fuels in a DTF. Costa et al. [28] investigated combustion kinetics and particle fragmentation of raw and torrified pine shells and olive stones in a drop tube furnace. Gas temperature, particle burnout and particle matter concentrations are measured for biomass fuels at different furnace temperatures in this study. Ndibe et al. [29] researched combustion, cofiring and emission characteristics of torrefied biomass in a drop tube furnace. In this study, cofiring characteristics of biomass are investigated. Also, combustion reactivity, emissions and burn-out are evaluated with measurements performed. Branco and Costa [30] researched effect of particle size on the burnout and emissions of particulate matter from the combustion of pulverized agricultural residues. In this work, temperature, particle burn-out and particulate matter concentration are measured for wheat straw and rice husk in a drop tube furnace. Zellagui et al. [31] studied the fast pyrolysis of woody biomass in a drop tube furnace at different temperatures and under two atmospheres. Wang et al. [32] studied the combustion characteristics of five biomass fuels and coal in a DTF. Data for gas temperatures, particle burnout and carbon, hydrogen, oxygen release along the reactor for these fuels are obtained by using drop tube furnace. Wang et al. [33] researched effect of biomass (straw and wood) co-firing with coal on NO_x emission and combustion efficiency in a DTF.

2.2 CFD Modelling of Drop Tube Furnaces

There are several studies for CFD modelling of drop tube furnaces in the literature. In this section, these studies are introduced.

Visona and Stanmore [34], Schönenbeck et al. [35] and Jones et al. [36] used laminar flow model for CFD analysis of drop tube furnace. Visona and Stanmore [34] performed modeling nitric oxide formation under laminar flow conditions in a drop tube furnace burning pulverized coal by using CFD. Schönenbeck et al. [35] studied NO-char reaction in the temperature range 1273-1573 K in a drop tube furnace. Laminar flow model is employed according to the results of Reynolds number calculation in this study. Jones et al. [36] performed a comprehensive biomass combustion model. Two fuels are employed. These fuels are wheat straw and bituminous coal. The combustion behaviours of these fuels are examined by using laminar flow CFD model in a DTF.

Feron [37], Zhang et al. [38], Jassim [39], Hart et al. [40], Wang [41] and Fan et al. [42] employed turbulence models in their studies. Feron [37] studied numerical and experimental characterization of a drop tube furnace and ash deposition analysis. Turbulence models are used according to the calculation of Grashof number, 10^{10}. k-ε and k-ω turbulence models are utilized in this study. CFD results obtained for temperature and velocity magnitudes inside the drop tube furnace are compared with the experimental results. This study reveals that the flow is driven in the drop tube furnace by natural convection. OpenFoam software is used for the analyses. Drop Tube Furnace schematic view, simulation and experimental results for [37] are presented in Figure 2.1 and Figure 2.2. Axial direction for temperature results is from bottom wall to upper wall in [37]. 6 m for the axial position is the entrance of the reactor. The results of simulations in this study highlight a sharp rise in temperature when the fluid enters in the DTF.

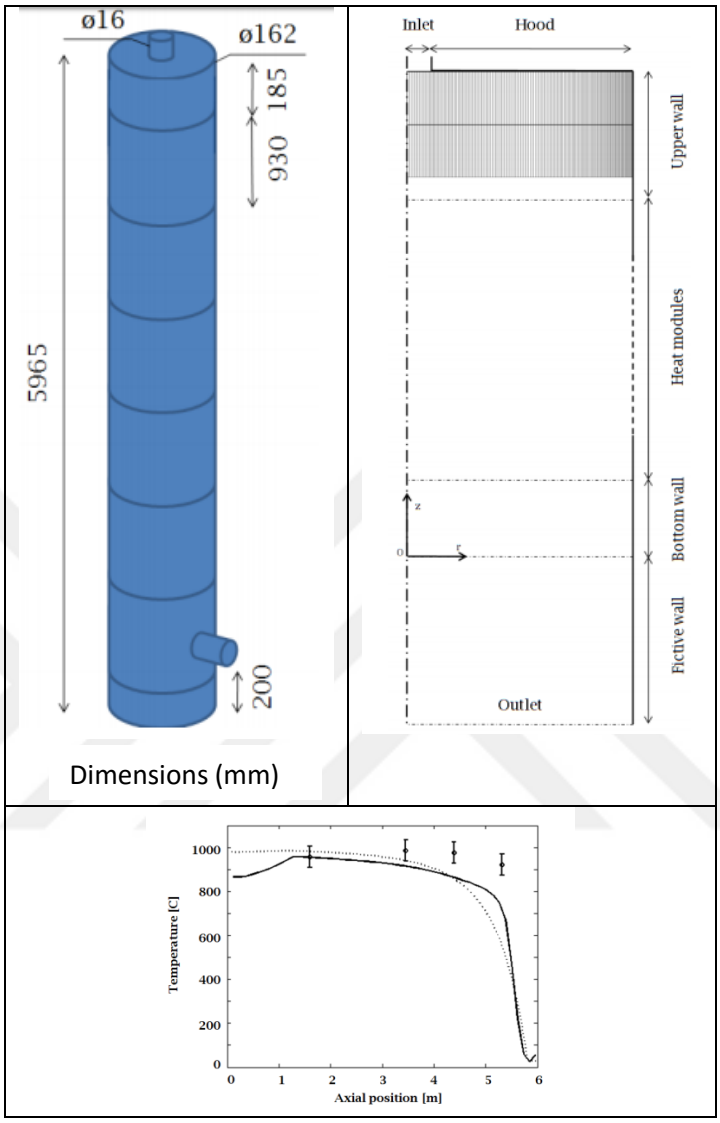

Figure 2.1 Drop Tube Furnace and Temperature Distribution [37] (circles-measured, solid line- simulations, dotted line – calculated)

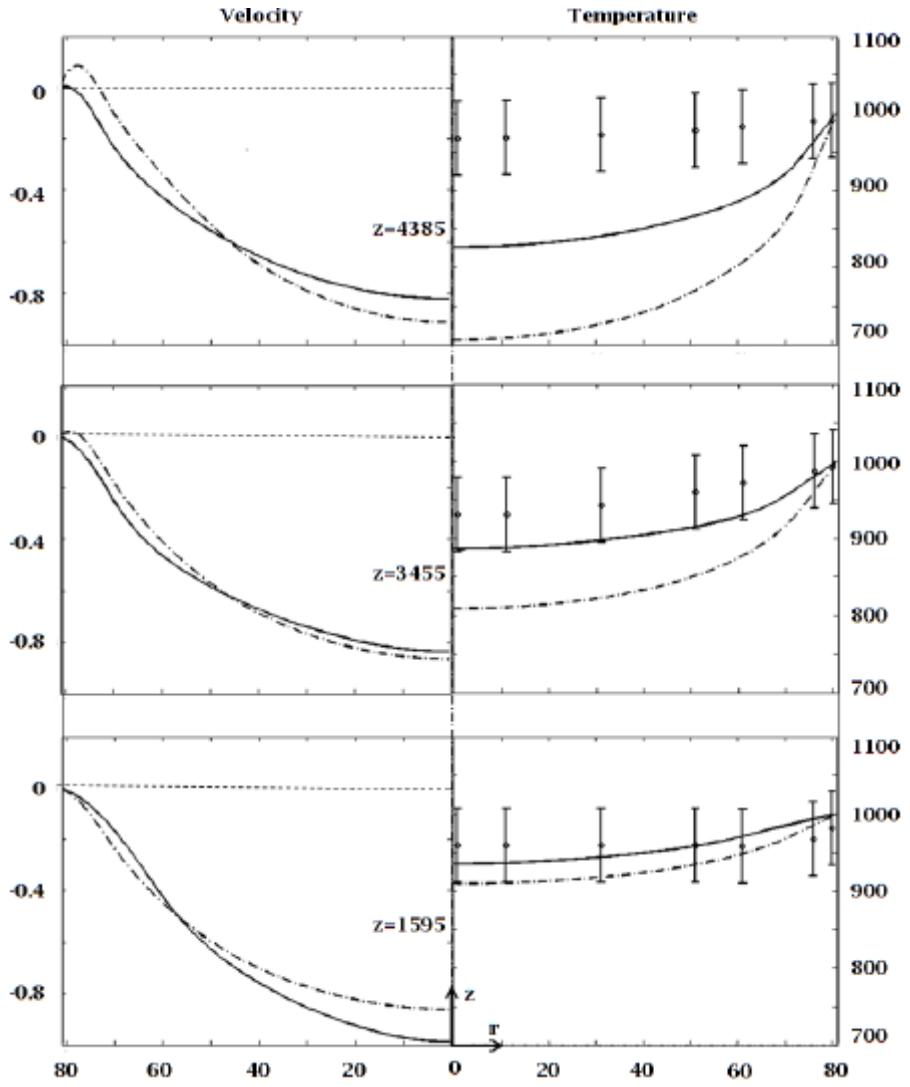

Figure 2.2 Radial Velocity (m/s) and Temperature (°C) Results in Different Axial Positions (mm) at T_{wall}= 1000 °C [37] (solid line-k-ε model, dash dotted line-k-ω model, circles-measurements and uncertainty)

Zhang et al. [38] employed CFD models for the investigation of the oxy-fuel combustion of Victorian brown coal in DTF. In this study, the oxy-fuel combustion characteristics of Victorian brown coal in a lab-scale drop tube furnace is evaluated by using 3D models of the reactor. Realizable k-ε model is employed as gaseous turbulence model. Particle temperature, volatile release, and char oxidation rate are obtained in this study.

Jassim [39] studied the behaviour of arsenic released during combustion of pulverized coal inside a DTF. 3D model is employed for the drop tube furnace. In this study, k-ε turbulence model, eddy dissipation model for the gas mixture phase, and discrete transfer model for particle radiation are used. Temperature profiles, flow stream pattern near inlets, mass fractions of CO, CO_2, As and As_2O_3 are obtained. The simulations are performed to study the evolution and vaporization of arsenic as a trace element for this work. Drop tube furnace used in this work and model created for the simulations are presented in Figure 2.3.

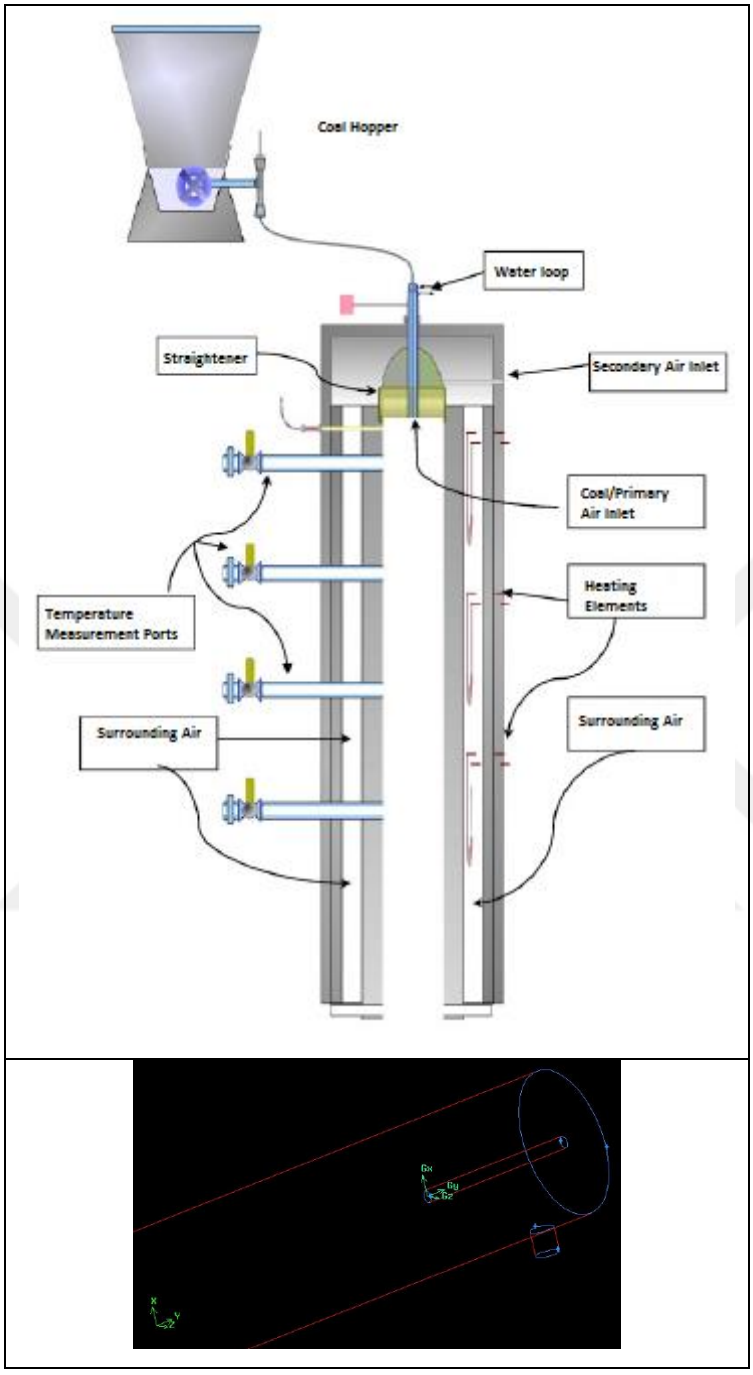

Figure 2.3 Drop Tube Furnace and Model Created for CFD [39]

Hart et al. [40] conducted a numerical study of pyrolysis of a Loy Yang coal in a pressurised drop tube furnace. An isothermal flow through the drop tube furnace is presented. k-ε model is used in this work.

Wang [41] studied solid fuel combustion with experiments and modelling. Matlab code and FLUENT software are employed for CFD modelling of the drop tube furnace in this study. The maximum temperature for the drop tube reactor is 1100 ° C. The length of cylinder tube is 1300 mm. In this work, the flow is not expected to be laminar due to sudden expansion regime and initial mixing between the particle loaded and the surrounding air. Therefore, k-ε model is employed with low inlet turbulent kinetic energy. Moreover, Discrete Ordinates Radiation, Species-Transport and Discrete Phase models are used for the simulations. Particle burnout and temperature distribution are obtained in this study. Drop tube furnace and temperature distribution along the centreline obtained in this study are given in Figure 2.4.

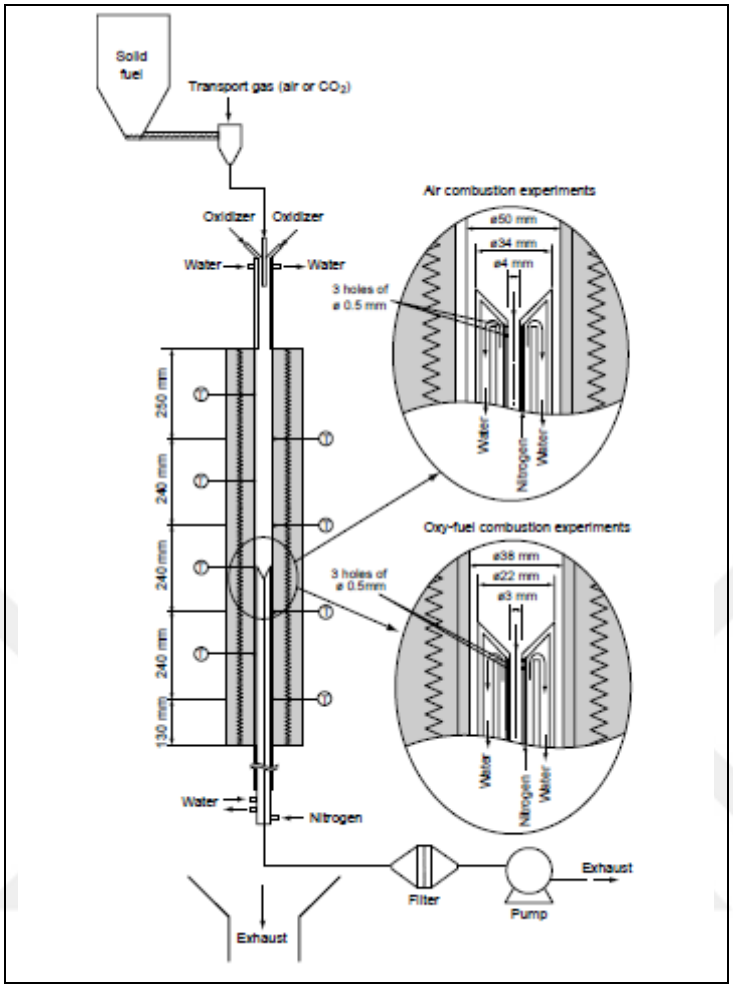
Solid fuel
Transport gas (air or CO_2)
Oxidizer
Oxidizer
Water
Water
3 holes of ø 0.5 mm
Air combustion experiments
ø50 mm
ø34 mm
ø4 mm
Water
Nitrogen
Water
250 mm
240 mm
240 mm
240 mm
130 mm
Oxy-fuel combustion experiments
3 holes of ø 0.5mm
ø38 mm
ø22 mm
ø3 mm
Water
Nitrogen
Water
Water
Nitrogen
Filter
Pump
Exhaust
Exhaust

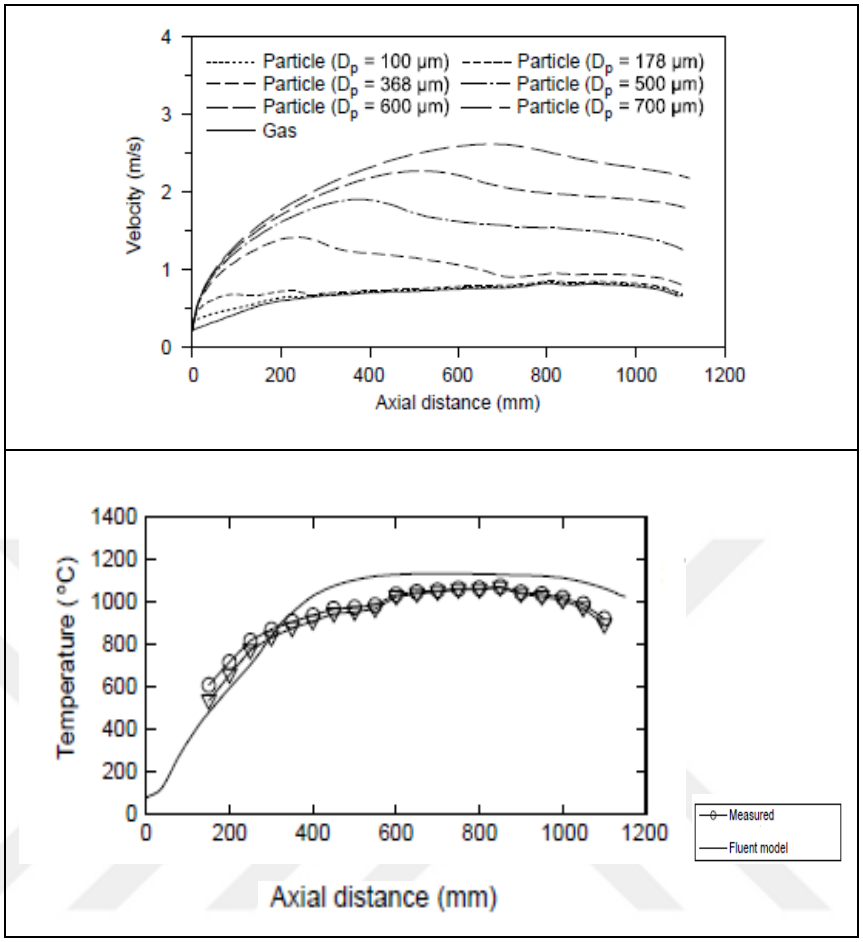

Figure 2.4 Drop Tube Furnace, Velocity Magnitudes and Temperature Distribution [41]

Fan et al. [42] studied simulation of the hydrogen reduction rate of magnetite concentrate particles in a drop tube furnace with CFD models. Gas temperature, particle temperature and residence time are obtained inside the reactor in the study. Realizable k-ε model is employed in the study. Figure 2.5 demonstrates drop tube furnace used for experiments and analysed in this study. Also, experimental and CFD results are presented for gas and particle temperature obtained in Figure 2.5.

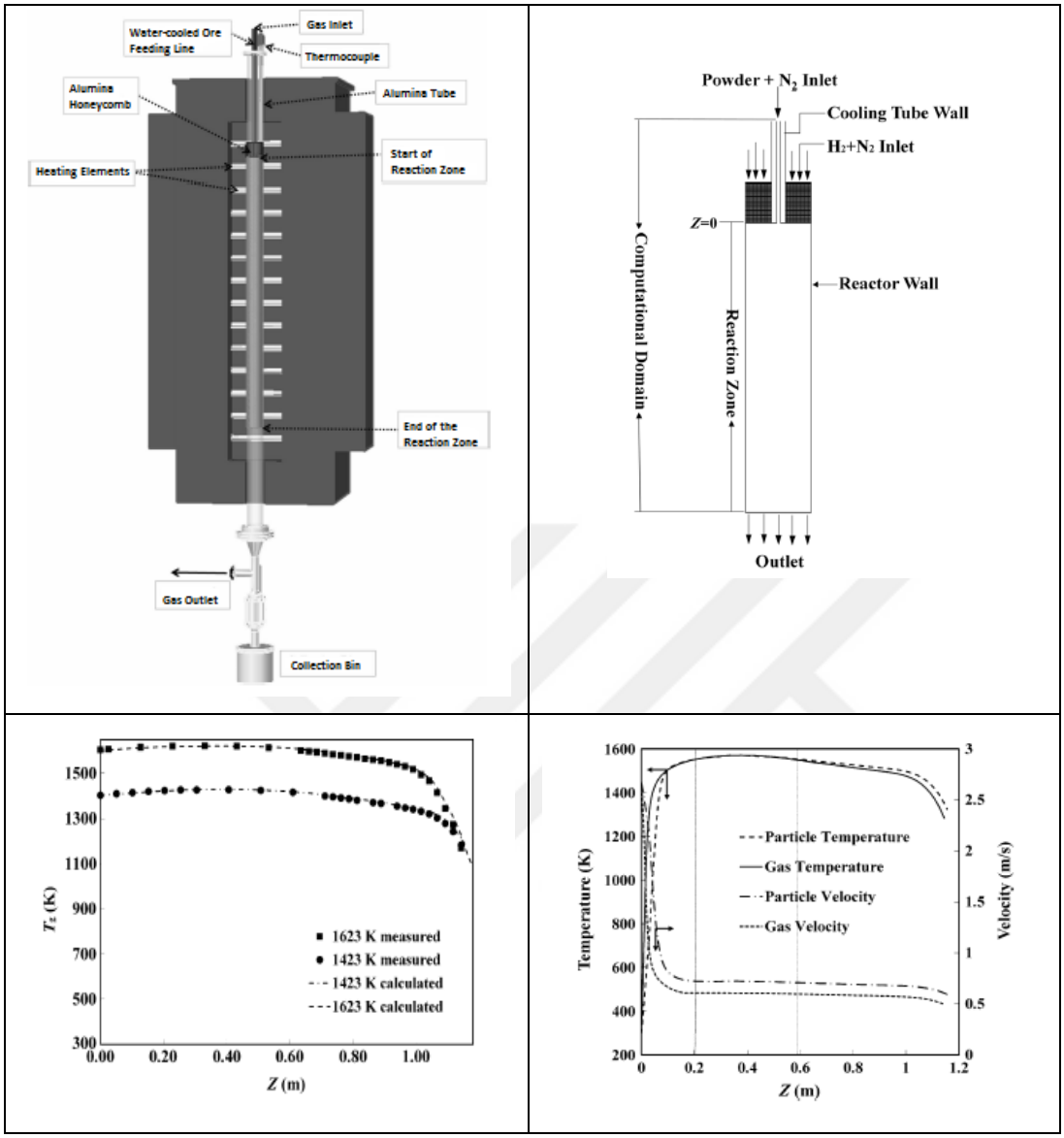

Figure 2.5 Drop Tube Furnace and Temperature Result [42]

Turbulence models used for drop tube furnace studies in literature are demonstrated in Table 2.1. Realizable or Standard k-ε models are employed in the literature.

Table 2.1 Turbulence Models Used for Drop Tube Furnace Studies

Study	Turbulence Model
Feron [37]	k-ε, k-ω models
Zhang et al. [38]	k-ε model
Jassim [39]	k-ε model
Hart et al. [40]	k-ε model
Wang et al. [41]	k-ε model
Fan et al. [42]	k-ε model

CHAPTER 3

NUMERICAL CHARACTERIZATION

In this chapter, firstly, the drop tube furnace analysed in the study is described. In order to validate numerical temperature findings of the DTF, temperature measurement is conducted. The details of the measurement performed in Clean Combustiın Technologies Laboratory and necessary corrections on the obtained data are outlined. Afterwards, numerical characterization of the flow inside the drop tube furnace is introduced in detail. Non-dimensional parameters are calculated at first. Then the geometry and mesh constructions generated in this study are described. Solver settings are presented for the flow simulations. FLUENT is employed as solver for the flow simulations of the drop tube furnace.

3.1 Drop Tube Furnace Experimental Rig Analysed in the Study

Drop Tube Furnaces are employed in order to reflect pulverized combustion systems. A drop tube furnace was built prior to this study in Clean Combustion Technologies Laboratory located in Department of Mechanical Engineering at Middle East Technical University for the investigation of pulverized combustion behaviours of co-firing various Turkish lignite coals with a variety of biomass fuels. Combustion experiments, such as validation of kinetic models, assessment of the particle burnout, analysis of the ash behaviour and particulate matter (PM) emissions can be conducted in this DTF.

The main parts of the drop tube furnace are the water-cooled injector, the feeding unit, the vertical alumina tube reactor, the heating elements, and the particle collection probe, as can be seen in Figure 3.1.

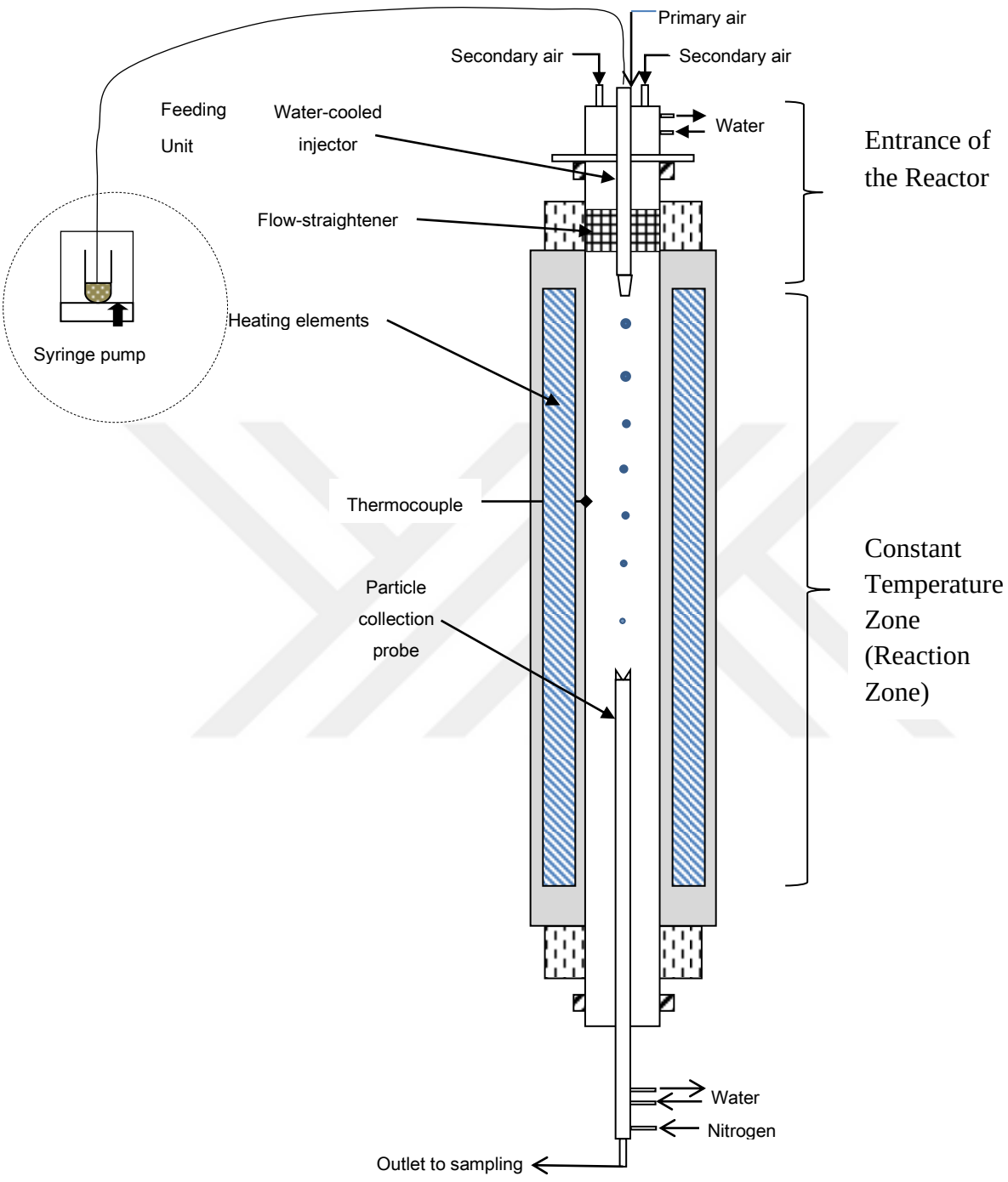

Figure 3.1 A Schematic View for the Drop Tube Furnace in the Clean Combustion Technologies Laboratory

Because drop tube furnaces are used to simulate real combustion systems, high temperature isothermal conditions should be provided. Therefore, the furnace is electrically heated by the heating elements. Only 1000 mm of the reactor is the heating zone (constant temperature zone, as shown in Figure 3.1) where the chemical reactions occur.

Drop Tube Furnaces are used for the pulverized fuel combustion. Hence, solid fuel should be pulverized. This system contains the vibration motor in order to pulverize the solid fuel. Pulverized fuel particles are inserted through a capillary tube from the injector. The water-cooled injector of the drop tube furnace has five inlets, as can be seen in Figure 3.2. While the primary air transports the fuel particles, the secondary air stream ensures sufficient oxygen for the combustion process. Particles are fed through the centre inlet of the injector. Secondary air enters the furnace through the remaining four inlets of the injector, as demonstrated in Figure 3.2. The overall view of the feeding unit and water-cooled injector systems is presented in Figure 3.3. Finally, burned particles are collected with the aid of a collection probe for sampling purposes.

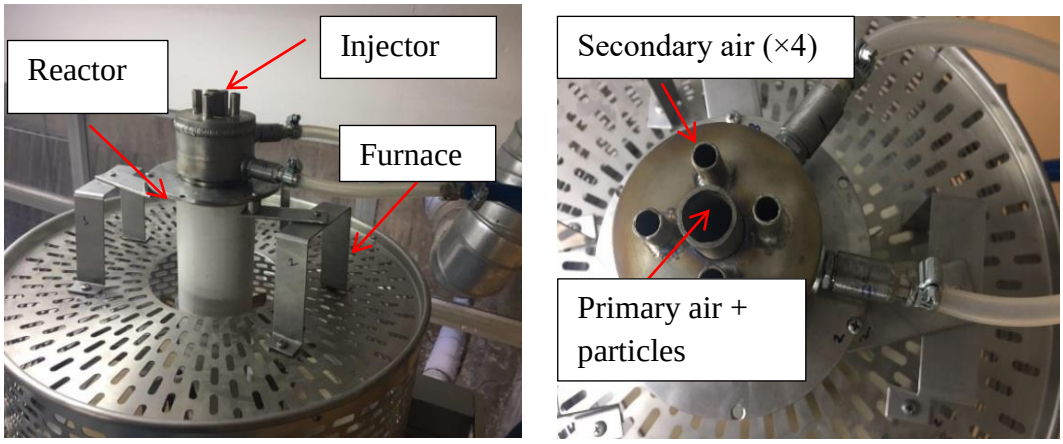

Figure 3.2 Water-cooled Injector

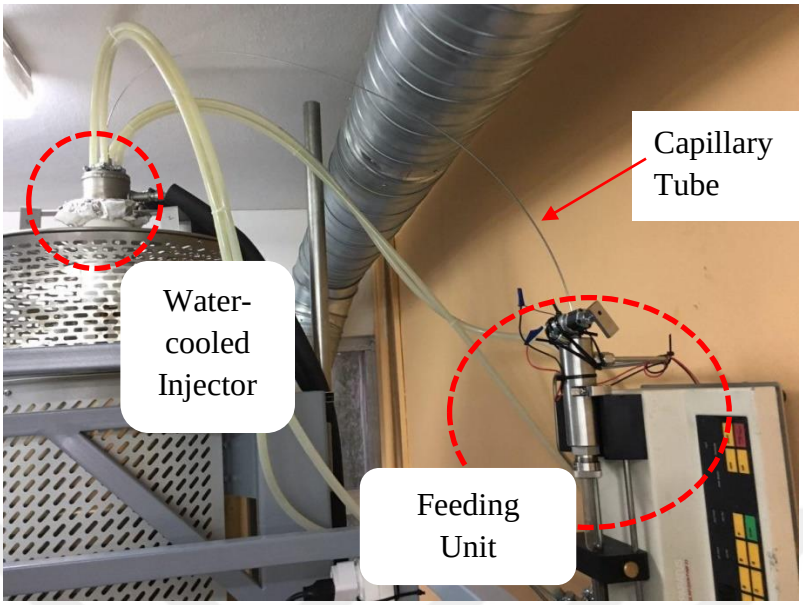

Figure 3.3 Feeding Unit and Water-cooled Injector

Total air volumetric flow rate entering the inlets was set as 10 L/min (lpm) for the experiments performed within the scope of the TÜBİTAK Career Award Project. 3 lpm air enters the primary air inlet, with diameter of 18 mm, and 7 lpm air enters the 4 secondary air inlets, with diameter is of 7 mm each. Velocity values for the primary and secondary air inlets are calculated as 0.196 m/s and 0.75 m/s, respectively, based on the equation shown under (3.1).

$$V = \frac{\dot{V}}{A} \tag{3.1}$$

The reactor (the heating zone – 1000 mm) is heated up to 1273 K during the experiments conducted within the scope of the TÜBİTAK project.

3.1.1 Experimental Temperature Data Collection Methodology

The temperature measurements are used for the validation of the analysis results in this study. The measurements are conducted along the centreline of the reactor from the injector tip. Average sampling time is 2 minutes per point inside the reactor. This time depends on the temperature fluctuations. Temperature should be approximately constant for each point.

The maximum temperature of the furnace is 1273 K. Therefore, the radiation coming from the heating elements may lead to temperature measurements distortion. The temperature measured with an exposed thermocouple is the gas temperature biased by the wall temperature with the effect of the radiation coming from the wall. The following equations, where T_g is the gas temperature, and T_{TC} is the thermocouple measured temperature, are given for the estimation of true gas temperatures. At steady state, neglecting conduction losses through the wires, the heat balance is formed between heat transfer to the thermocouple and radiation losses from the thermocouple [43].

$$q_c(convective\ heat\ transfer) = q_r(radiation\ heat\ transfer) \tag{3.2}$$

$$q_c = hA(T_g - T_{TC}) \tag{3.3}$$

$$q_r = \epsilon\sigma A(T_{TC}^4 - T_{TC,surr}^4) \tag{3.4}$$

Also assuming that the radiation transfer from the surrounding of the probe can be neglected, the result is that the difference between the true gas temperature and temperature ΔT is

$$\Delta T = T_g - T_{TC} = (\varepsilon\sigma T_{TC}^4)/h \tag{3.5}$$

Where the convective heat transfer coefficient is given as follows:

$$h = (\frac{k_c}{d})(2 + 0.6\left(\frac{c_p \mu}{k}\right)^{0.33} (\frac{Vd\rho}{\mu})^{0.5} \quad (3.6)$$

According to the calculations based on the equations from (3.2) to (3.6), the temperature difference between measured value and true gas temperature is approximately 10%. An example for the correction calculation is given in Appendix A.

3.2 Non-dimensional Parameters

In this section, non-dimensional parameters are calculated in order to determine the dominant phenomena leading to fluid motion and the flow regime type in the drop tube furnace. Reynolds, Prandtl, Grashof, and Rayleigh numbers are calculated within this scope at first. Afterwards, heat tranfer modes are described in furnaces and Nusselt number is calculated.

The DTF characteristics are shown in Table 3.1.

Table 3.1 The DTF Characteristics

L = heated zone length = 1 m
g = 9.81 m/s^2
d_1 = primary air inlet diameter = 18 mm
d_2 = secondary air inlets diameter = 7 mm
V_1 = primary air inlet velocity = 0.196 m/s
V_2 = secondary air inlet velocity = 0.75 m/s
T_w = wall temperature = 1273 K
T_∞ = air inlet temperature = 293 K

Reynolds number is the ratio of the inertia forces to viscous forces. Reynolds number is important for the regime of the fluid flow.

$$Re = \frac{\rho V D}{\mu} \tag{3.7}$$

Prandtl number indicates the ratio of the momentum diffusivity to thermal diffusivity.

$$Pr = \frac{\nu}{\alpha} \tag{3.8}$$

Prandtl number is approximately 0.7 for air [44].

Natural convection generates a fluid motion caused by the density differences in the fluid due to temperature gradient leading to a buoyancy force acting on the fluid. In natural convection situations, Grashof number is an important dimensionless number since it allows to determine the flow type, in similarity to the Reynolds number in forced convection. Grashof number calculates the ratio of the buoyancy to viscous force. Grashof number affects the type of the fluid flow. Therefore, Grashof number should be calculated in order to decide the regime of the fluid flow in case of natural convection. When Grashof number is higher than 10^9, the flow is turbulent [37].

Drop tube furnaces can be considered as vertical cylinder. Therefore, Gr_L formula is used for the calculation of Grashof number [37].

$$Gr = \frac{\beta \Delta T g L^3}{\nu^2} \tag{3.9}$$

$$T_{film} = \frac{T_w + T_\infty}{2} \tag{3.10}$$

The air properties should be calculated at T_{film} (783 K) for the calculation of Grashof number.

Natural convection occurs only inside the heating zone, because wall temperature of water-cooled injector is 293 K. In this case, natural convection will not occur inside the water-cooled injector.

Rayleigh number is a dimensionless number which is related to buoyancy-driven flow.

$$Ra = Gr \times Pr \tag{3.11}$$

The results for the dimensionless numbers are presented in Table 3.2.

Table 3.2 The Dimensionless Numbers

Re at the central inlet	Re at the secondary air inlets	Gr inside the heating zone	Ra inside the heating zone
233	347	1.99×10^{9}	1.39×10^{9}

Furthermore, Gr/Re^2 is calculated. Gr/Re^2 is a parameter which is a measure of the relative importance of natural convection in comparison with forced convection. Reynolds number should be calculated inside the heating zone for this parameter. However, velocity magnitude inside the heating zone is unknown at first. Therefore, the parameter is calculated approximately in the beginning. After the analysis results, the parameter is validated. On the other hand, it is estimated that Reynolds number is low due to low velocity inside the heating zone.

When $Gr/Re^2=1$, natural convection and forced convection are of the same order of magnitude.

When $Gr/Re^2<<1$, forced convection is dominant.

When $Gr/Re^2>>1$, natural convection is dominant. In this case, the buoyancy force governs the fluid motion [37].

In this thesis, natural convection is dominant inside the heating zone because of $Gr/Re^2>>1$. Also, the flow is turbulent due to Grashof number inside the heating zone. Due to the fact that the buoyancy forces are large relative to viscous forces, viscous forces cannot prevent the formation of rapid fluctuations of the fluid motion.

Drop Tube Furnaces are utilized in order to simulate the boilers. The three modes of heat transfer take place in a boiler furnace. Conduction occurs through the walls. Convection occurs due to the movement of the hot gases. Radiation generates from the flame, hot combustion products and the furnace walls. Heat transfer phenomena inside a typical furnace are schematically demonstrated in Figure 3.4.

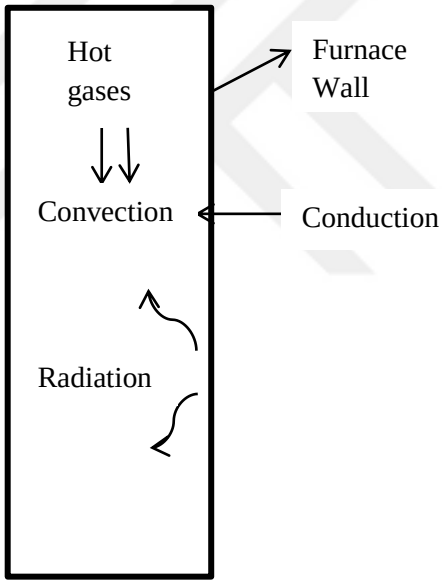

Figure 3.4 Heat Transfer in the Furnace

The simulations in this study are performed without calculating the fuel combustion. In this case, air is assumed as transparent. The transmissibility of the gas is equal to one for this assumption. Thus, the radiation is neglected. Natural convection is the dominant convection phenomena for the drop tube furnace analysed in this study according to the results of the dimensionless numbers. The reactor of the furnace in this work is electrically heated by the heating elements. Therefore, the constant temperature is selected as boundary condition for the walls.

The Nusselt number is the ratio of convective heat transfer to conductive heat transfer. Hence, the Nusselt number quantifies the relative importance of both heat transfer mechanisms for the flow. The convection is large relative to conduction for high Nusselt numbers. In case of natural convection, the Nusselt number is function of Grashof and Prandtl numbers [45].

The vertical cylinder is assumed as the vertical plate, when [45]

$$\frac{d}{L} \geq \frac{35}{Gr_L^{\frac{1}{4}}} \tag{3.12}$$

Due to the fact that this criterion is not provided for this study, the average heat transfer coefficient should be multiplied by a factor F [45].

$$F = 1.3[(\frac{L}{d})/Gr_d]^{1/4}+1.0 \tag{3.13}$$

F is calculated as 1.12 by using (3.13).

$$Nu_f = 0.10(Gr_L Pr_L)^{1/3} \tag{3.14}$$

$$\overline{Nu}^{1/2} = 0.825 + \frac{0.387Ra^{1/6}}{[1+(0.492/Pr)^{9/16}]^{8/27}} \quad 10^{-1} < Ra_L < 10^{12} \tag{3.15}$$

The Nusselt number is calculated as 124.99 and 131.264 from (3.14) and (3.15) respectively.

$$Nu = \frac{hL}{k} \tag{3.16}$$

By using equation (3.16), the heat transfer coefficient is calculated as 7.06 W/m^2.K and 7.42 W/m^2.Kwith the Nusselt numbers obtained from (3.14) and (3.15) respectively.

3.3 Computational Fluid Dynamics Analysis

In this section, computational domain and boundary conditions used for this study are described. Mesh parameters and solver settings are introduced for the flow simulations. Finally, the mathematical modelling for Computational Fluid Dynamics is presented.

3.3.1 Domain and Boundary Conditions

The water-cooled injector of the drop tube furnace analysed in this study has five inlets, as indicated in Figure 3.2. One of these inlets is at the centre of the injector, which provides primary air. Secondary air inlets (4 inlets) of the water-cooled injector, as can be seen in Figure 3.2, are of the same diameter. In addition, air enters these inlets at the same velocity. Furthermore, other boundary conditions (temperature, gravity etc.) have same effects on these inlets. The drop tube furnace has four symmetry surfaces. It is expected that the flow is almost the same at these symmetry surfaces, because both boundary conditions and the geometry are symmetrical on these surfaces. Although there is natural convection and turbulent flow inside the drop tube furnace, these factors are not expected to change the symmetry significantly. Moreover, the quarter model will be enough to investigate temperature and velocity magnitude results aimed to be obtained in this study. In addition, even the assumption of a 2D axisymmetric computational domain is enough for drop tube furnaces in which flow does not show any important variation in the azimuthal direction [46]. In literature, simplified model was created for analysing the drop tube furnace, as indicated in Figure 2.3. Consequently, simplified quarter model is developed and used in order to decrease computational time in this study, as can be seen in Figure 3.5.

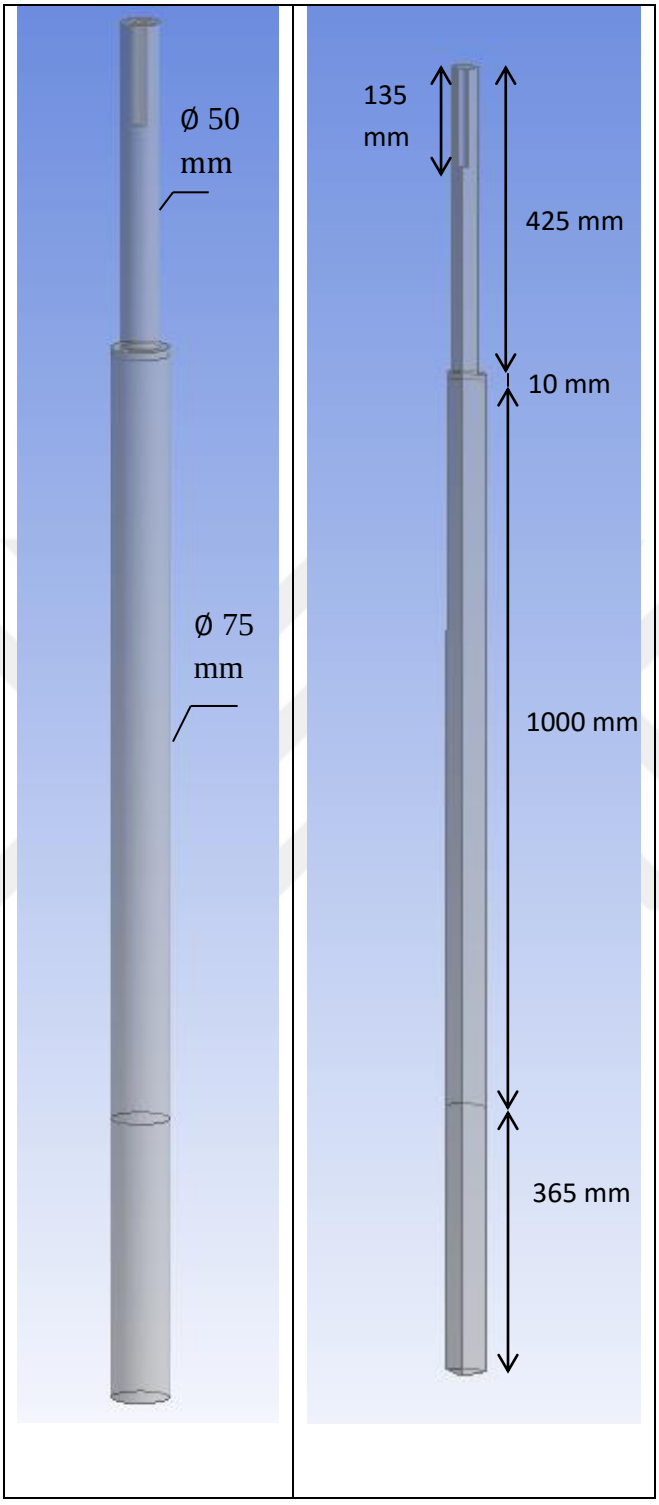

Figure 3.5 Full Model, 1/4 Model and Dimensions for the Drop Tube Furnace

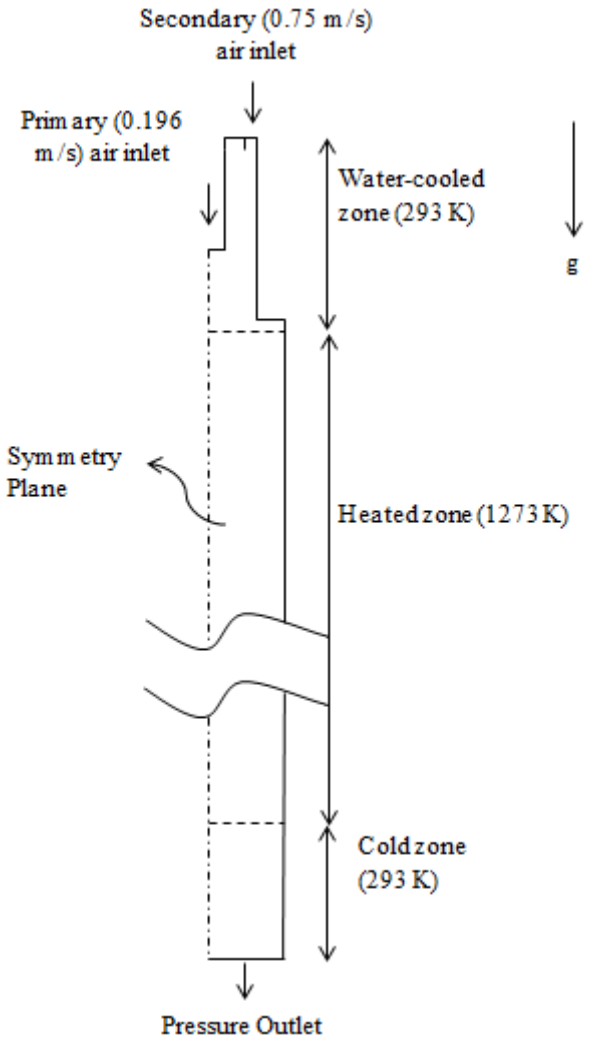

Figure 3.6 A Typical Computational Domain Used in This Study

A typical computational domain used in this study is demonstrated in Figure 3.6. The boundary conditions in Figure 3.6 are employed for the simulations.

Moreover, as fuel combustion is not taken into account in the analyses, the fluid flow inside the furnace is assumed to be air. Air properties are temperature-dependent, therefore air properties should be defined as a function of the temperature. The density is defined as incompressible ideal gas. Specific heat capacity and thermal conductivity are defined as polynomial function. Sutherland Law is selected for viscosity. More detailed information about air properties is indicated in Appendix B.

3.3.2 Mesh Parameters and Solver Settings

The structured mesh which contains 3D hexahedral elements is generated. The mesh is crucial for obtaining the accurate results and good convergence. The structured mesh types are mostly preferred for natural convection analyses because of their high quality. On the other hand, structured mesh types are not applicable for complicated faces. Because of the fact that the model in this study contains simple faces, the structured mesh is applicable for the purpose of this study. The different meshes are created for the mesh independence study, as can be seen in Table 3.3. After the meshes are created, y^+ values are checked. y^+ values should be lower than 1 for SST k-ω model. The meshes generated in this study have acceptable mesh quality. Standard k-ε model is employed for the mesh independence study. Mesh independence study is carried out to confirm that the solutions are independent of element number.

Table 3.3 Mesh Independence Study

	Coarse Mesh	Medium Mesh	Fine Mesh
Elements	275169	603608	1568730
Maximum Skewness	0.52	0.49	0.58

The natural convection simulations are difficult analyses to obtain good convergence, because density varies with temperature. Boussinesq model should be used for steady-state calculations in natural convection case, because Boussinesq model provides fast and good convergence. On the other hand, Boussinesq approximation is valid only in small temperature differences in the domain. In Boussinesq model, density is specified as approximately constant [47].

Boussinesq approximation;

$$(\rho-\rho_0)g \approx \rho_0\beta(T-T_0)g \tag{3.17}$$

However, there are large temperature differences in the domain for this study. Hence, Boussinesq approximation is not valid for this thesis. In case of large temperature differences, transient analysis should be used to achieve convergence.

The flow type is evaluated for the inlets in which there are sudden expansions. The flow is laminar for inlet Reynolds number below 200 [41]. In this thesis, Reynolds numbers at inlets are above 200, as can be seen in Table 3.2. Hence, the flow type for inlets is considered as turbulent flow with low inlet turbulent kinetic energy, as shown under (3.18).

$$k = \frac{3}{2}(UI)^2 \tag{3.18}$$

Moreover, the flow is turbulent based on the Grashof number ($Gr>10^9$) inside the heated zone. Therefore, standard k-ε, realizable k-ε and SST k-ω models are used for natural convection simulations. Whereas steady-state approximation is used for the solutions with k-ε models, transient solution is employed for SST k-ω model to achieve convergence, because the analysis in which SST k-ω model is used is not converged with steady-state solution. Time-dependent approach should be used to achieve convergence in this case [47]. Time-average results are obtained for the analysis in which SST k-ω model is utilized in order to compare steady k-ε models results . Flow analysis using SST k-ω model is solved during 25 seconds based on the residence time and oscillations.

The scaled residuals values are employed to check the convergence behaviour. The scaled residuals, as can be seen in Figure 3.7, are set as 10^{-6} for continuity, momentum equations and as 10^{-9} for energy equation of the simulations using k-ε model. However, the scaled residuals are set as 10^{-6} for continuity, momentum equations and as 10^{-8} for energy equation of the simulations using k-ω model in order to decrease the computational time. In addition, the temperature and velocity magnitudes are plotted on the monitor points. The trends of the sample monitor points (the entrance and the exit of the heated zone) in the analysis using Standard k-ε model are demonstrated in Figures 3.8 and 3.9.

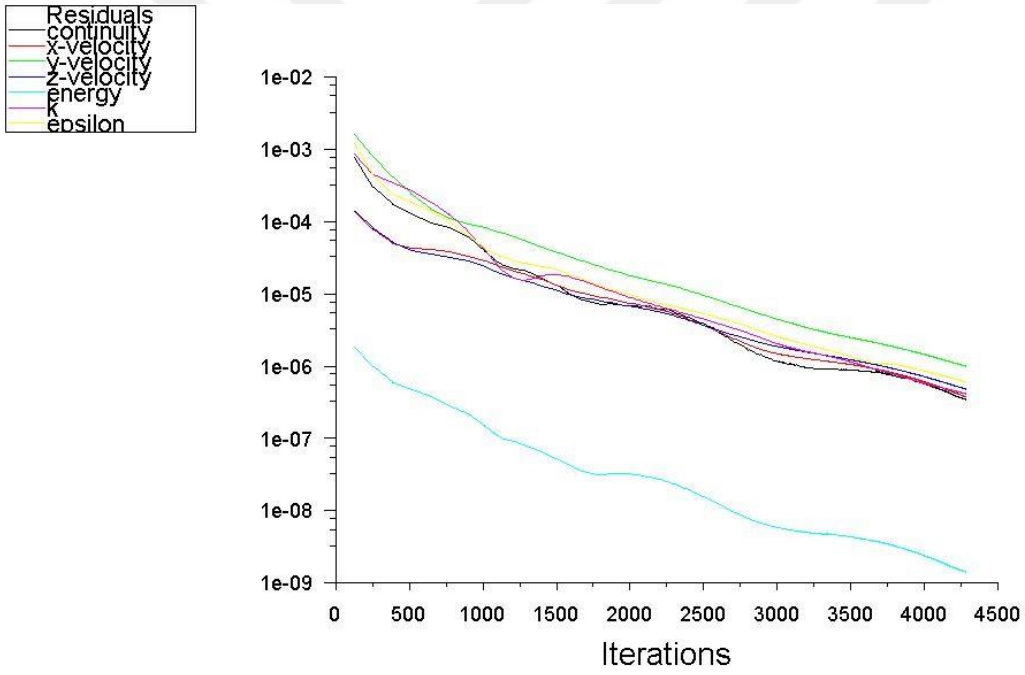

Figure 3.7 Convergence history for a typical simulation performed by using standard k-ε model in this study

a)

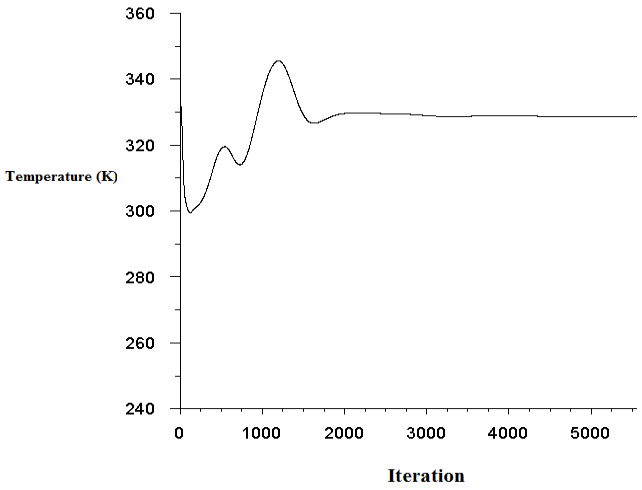

b)

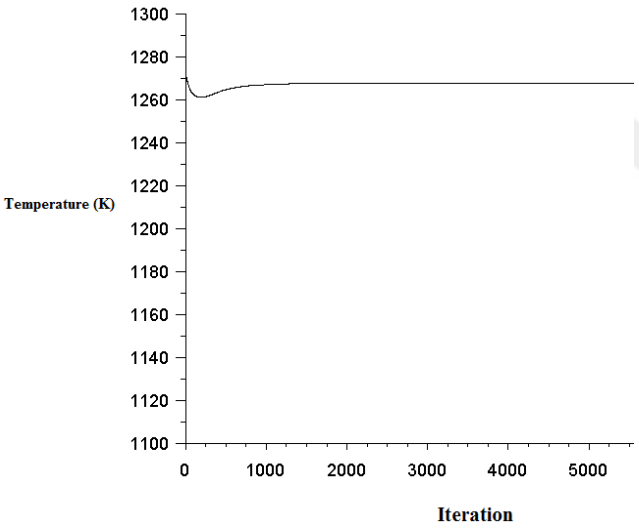

Figure 3.8 Sample monitor point results for temperature (K) a) at the entrance of the heated zone centreline, b) at the exit of the heated zone centreline

a)

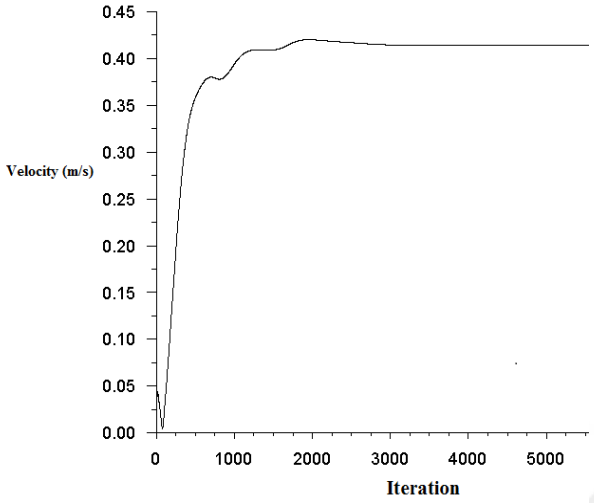

b)

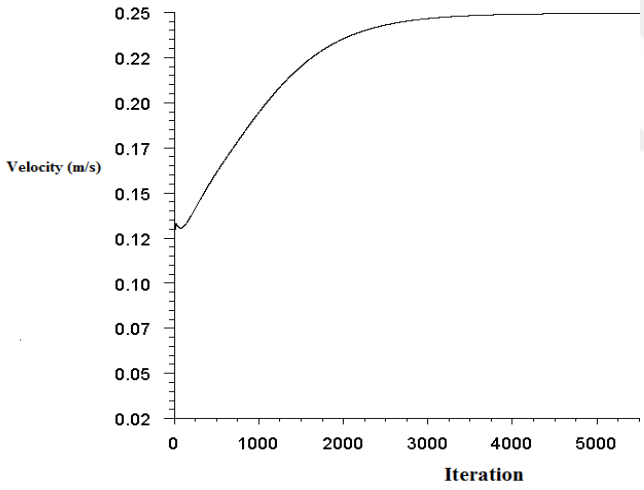

Figure 3.9 Sample monitor point results for velocity (m/s) a) at the entrance of the heated zone centreline, b) at the exit of the heated zone centreline

Table 3.4 Solver Settings Used in FLUENT

	Steady-State		Unsteady
Viscous Model	Laminar	Standard k-ε Realizable k-ε	SST k-ω
Pressure-Velocity Coupling Scheme	SIMPLE	SIMPLE	SIMPLE
Gradient Discretization	Least Squares Cell Based	Least Squares Cell Based	Least Squares Cell Based
Pressure Discretization	Standard	PRESTO	PRESTO
Momentum Discretization	Second Order	Second Order	Second Order
Energy Discretization	Second Order	Second Order	Second Order
Turbulent Kinetic Energy Discretization	Second Order	Second Order	Second Order
Specific Dissipation Rate Discretization	Second Order	Second Order	Second Order

The solver settings used in FLUENT are presented in Table 3.4. Due to the fact that second order scheme improves the accuracy, second order scheme is utilized for the simulations. Standard scheme in FLUENT is mostly enough for analyses. However, PRESTO! scheme which uses the discrete continuity balance for a staggered control volume about the face to compute the staggered pressure should be employed for high Rayleigh number ($Ra>10^8$) natural convection analysis [47]. When pressure-based solver is employed, PRESTO! should be used as pressure interpolation scheme for natural convection analyses in order to obtain better convergence. Hence, PRESTO! is selected as pressure interpolation scheme for natural convection analyses in this thesis. Because of the fact that Least Squares Cell-Based is appropriate choice for structured mesh, Least Squares Cell-Based method is employed in this study.

3.3.3 Mathematical Modelling

In this part, governing equations of fluid flow and transport equations for turbulence models (Standard k-ε, Realizable k-ε, and SST k-ω) are presented respectively.

3.3.3.1 Governing Equations of Fluid Flow

The general form of instantaneous governing equations for compressible Newtonian fluid is given as follows [48]:

Continuity: $$\frac{\partial \rho}{\partial t} + \nabla . \left(\rho \vec{V}\right) = 0 \quad (3.19)$$

x-momentum: $$\frac{\partial (\rho u)}{\partial t} + \nabla . \left(\rho u \vec{V}\right) = -\frac{\partial P}{\partial x} + \frac{\partial \tau_{xx}}{\partial \mathrm{x}} + \frac{\partial \tau_{yx}}{\partial y} + \frac{\partial \tau_{zx}}{\partial z} + \rho f_x \quad (3.20)$$

y-momentum: $$\frac{\partial (\rho v)}{\partial t} + \nabla . \left(\rho v \vec{V}\right) = -\frac{\partial P}{\partial y} + \frac{\partial \tau_{xy}}{\partial \mathrm{x}} + \frac{\partial \tau_{yy}}{\partial y} + \frac{\partial \tau_{zy}}{\partial z} + \rho f_y \quad (3.21)$$

z-momentum: $$\frac{\partial (\rho w)}{\partial t} + \nabla . \left(\rho w \vec{V}\right) = -\frac{\partial P}{\partial z} + \frac{\partial \tau_{xz}}{\partial \mathrm{x}} + \frac{\partial \tau_{yz}}{\partial y} + \frac{\partial \tau_{zz}}{\partial z} + \rho f_z \quad (3.22)$$

Energy: $$\frac{\partial (\rho e)}{\partial t} + \nabla . \left(\rho e \vec{V}\right) = -p \nabla . \vec{V} + \nabla . (k \nabla T) + \Phi + q \quad (3.23)$$

Equation of State: $$P = \rho R T \quad (3.24)$$

In these equations, V represents the velocity vector and u, v and w are the velocity components in the x, y and z directions respectively. ρ represents the density, p is pressure, f_x, f_y and f_z are the body forces, R is the gas constant, e is the internal energy, k is the thermal conductivity, and q is the heat flux as a source term.

τ is the viscous stress which can be defined for the Newtonian fluids as:

$$\tau_{xx} = \lambda\left(\frac{\partial u}{\partial x} + \frac{\partial v}{\partial y} + \frac{\partial w}{\partial z}\right) + 2\mu\frac{\partial u}{\partial x} \tag{3.25}$$

$$\tau_{yy} = \lambda\left(\frac{\partial u}{\partial x} + \frac{\partial v}{\partial y} + \frac{\partial w}{\partial z}\right) + 2\mu\frac{\partial v}{\partial y} \tag{3.26}$$

$$\tau_{zz} = \lambda\left(\frac{\partial u}{\partial x} + \frac{\partial v}{\partial y} + \frac{\partial w}{\partial z}\right) + 2\mu\frac{\partial w}{\partial z} \tag{3.27}$$

$$\tau_{xy} = \tau_{yx} = \mu\left(\frac{\partial u}{\partial y} + \frac{\partial v}{\partial x}\right) \tag{3.28}$$

$$\tau_{xz} = \tau_{zx} = \mu\left(\frac{\partial u}{\partial z} + \frac{\partial w}{\partial x}\right) \tag{3.29}$$

$$\tau_{zy} = \tau_{yz} = \mu\left(\frac{\partial w}{\partial y} + \frac{\partial v}{\partial z}\right) \tag{3.30}$$

Where μ represents the dynamic viscosity and λ is the second viscosity coefficient. The second viscosity coefficient is approximately given by Stokes in Equation 3.31.

$$\lambda = -\frac{2}{3}\mu \tag{3.31}$$

In the energy equation, as shown under (3.23), Φ is the viscous dissipation term which impacts the dissipation of mechanical energy into heat. Due to the fact that this term is usually very small except for high Mach numbers, it is neglected.

$$\Phi = \lambda(\nabla.\vec{V})^2 + \mu\left[2\left(\frac{\partial u}{\partial x}\right)^2 + 2\left(\frac{\partial v}{\partial y}\right)^2 + 2\left(\frac{\partial w}{\partial z}\right)^2 + \left(\frac{\partial u}{\partial y} + \frac{\partial v}{\partial x}\right)^2 + \left(\frac{\partial u}{\partial z} + \frac{\partial w}{\partial x}\right)^2 + \left(\frac{\partial w}{\partial y} + \frac{\partial v}{\partial z}\right)^2\right] \tag{3.32}$$

3.3.3.2 Turbulence Models

The flow is turbulent inside the drop tube reactor due to natural convection phenomena ($Gr>10^9$). Hence, a suitable turbulence model is needed to be defined. The turbulence models used for this study are identified based on the studies in literature, as can be seen in Table 2.1. The selected turbulence models are standard k-ε, realizable k-ε and k-ω SST models. In this section, the equations solved for turbulence models are provided as follows:

k-ε models solve transport equations for k and ε.

Transport equations for standard k-ε model:

$$\frac{\partial(\rho k)}{\partial t}+\frac{\partial(\rho k u_i)}{\partial x_i}=\frac{\partial}{\partial x_j}\left[\left(\mu+\frac{\mu_t}{\sigma_k}\right)\frac{\partial k}{\partial x_j}\right]+G_k+G_b-\rho\varepsilon-Y_M+S_k \tag{3.33}$$

$$\frac{\partial(\rho \varepsilon)}{\partial t}+\frac{\partial(\rho \varepsilon u_i)}{\partial x_i}=\frac{\partial}{\partial x_j}\left[\left(\mu+\frac{\mu_t}{\sigma_\varepsilon}\right)\frac{\partial \varepsilon}{\partial x_j}\right]+C_{1\varepsilon}\frac{\varepsilon}{k}(G_k+C_{3\varepsilon}G_b)-C_{2\varepsilon\rho}\frac{\varepsilon^2}{k}+S_\varepsilon \tag{3.34}$$

$$\mu_t=C_\mu\rho\frac{k^2}{\varepsilon} \tag{3.35}$$

In equations from 3.33 to 3.35, G_k impacts the generated kinetic energy from the mean velocity gradient. G_b shows turbulence kinetic energy generated with buoyancy effect. Y_M demonstrates the fluctuating dilatation in compressible turbulence. $C_{1\varepsilon}$, $C_{2\varepsilon}$ and $C_{3\varepsilon}$ are constants. σ_k and σ_ε are the turbulent Prandtl numbers for k and ε, respectively. S_k and S_ε are user-defined source terms.

Transport Equations for realizable k-ε model,

$$\frac{\partial(\rho k)}{\partial t} + \frac{\partial(\rho k u_j)}{\partial x_j} = \frac{\partial}{\partial x_j}\left[\left(\mu + \frac{\mu_t}{\sigma_k}\right)\frac{\partial k}{\partial x_j}\right] + G_k + G_b - \rho\varepsilon - Y_M + S_k \tag{3.36}$$

$$\frac{\partial(\rho\varepsilon)}{\partial t} + \frac{\partial(\rho\varepsilon u_j)}{\partial x_j} = \frac{\partial}{\partial x_j}\left[(\mu + \frac{\mu_t}{\sigma_\varepsilon}\frac{\partial\varepsilon}{\partial x_j}\right] + \rho C_1 S_\varepsilon - \rho C_2 \frac{\varepsilon^2}{k+\sqrt{v\varepsilon}} C_{1\varepsilon}\frac{\varepsilon}{k} C_{3\varepsilon} G_b + S_\varepsilon \tag{3.37}$$

$$C_1 = \max\left[0.43, \frac{n}{n+0.5}\right], n = S\frac{\varepsilon}{k}, S = \sqrt{2S_{ij}S_{ij}} \tag{3.38}$$

$$\mu_t = C_\mu \rho \frac{k^2}{\varepsilon} \tag{3.39}$$

In equations from 3.36 to 3.39, G_k impacts the generated kinetic energy due to mean velocity gradient. G_b shows turbulence kinetic energy generated with buoyancy effect. Y_M demonstrates the fluctuating dilatation in compressible turbulence. C_1, C_2 and $C_{3\varepsilon}$ are constants. σ_k and σ_ε are the turbulent Prandtl numbers for k and ε, respectively. S_k and S_ε are user-defined source terms.

The Shear-Stress Transport (SST) k-ω model solves transport equations for k and ω.

$$\frac{\partial(\rho k)}{\partial t} + \frac{\partial(\rho k u_i)}{\partial x_i} = \frac{\partial}{\partial x_j}\left[\Gamma_k \frac{\partial k}{\partial x_j}\right] + G_k - Y_k + S_k \tag{3.40}$$

$$\frac{\partial(\rho w)}{\partial t} + \frac{\partial(\rho w u_i)}{\partial x_i} = \frac{\partial}{\partial x_j}\left[\Gamma_w \frac{\partial w}{\partial x_j}\right] + G_w - Y_w + D_w + S_w \tag{3.41}$$

$$\Gamma_k = \mu + \frac{\mu_t}{\sigma_k} \tag{3.42}$$

$$\Gamma_w = \mu + \frac{\mu_w}{\sigma_w} \tag{3.43}$$

$$\mu_t = \frac{\rho k}{w} \frac{1}{\max\left[\frac{1}{a'}, \frac{SF_2}{a_1 w}\right]} \tag{3.44}$$

In above equations, G_k impacts the generated turbulent kinetic energy due to the mean velocity gradient. Γ_w, Γ_k represent the turbulent diffusivity of w and k respectively. Y_w and Y_k demonstrate the fluctuating dilatation in compressible turbulence. S_k and S_w are used-defined source terms, D_w is the cross-diffusion term and G_w shows the generation of w.

CHAPTER 4

RESULTS AND DISCUSSIONS

In this chapter, the mesh independence study is introduced at first. Afterwards, temperature distribution solutions in which three different models (standard k-ε, realizable k-ε, and SST k-ω) are utilized are presented. The results obtained from CFD simulations are compared with both the measurements performed in the drop tube furnace and the analysis results of similar studies in literature. Thus, the suitable model for this study is investigated. Then velocity magnitudes inside the furnace are presented. Finally, gravitational effect is analysed on the flow in the DTF.

4.1 Mesh Independence Study

Three different mesh constructions are generated in order to study mesh independence. The numbers of elements are 275169, 603608, and 1568730 from the coarse mesh to the fine mesh respectively, as can be seen in Table 3.3. Standard k-ε model is employed for the mesh independence study. Temperature and velocity magnitudes obtained by using three different meshes are compared in Figure 4.1 and Figure 4.2. As seen in the figures, the results obtained with three different meshes are very similar except some points. Due to the fact that the results obtained with three different meshes are close to each other, medium mesh is considered as appropriate and sufficient for the CFD simulations of the DTF in this thesis.

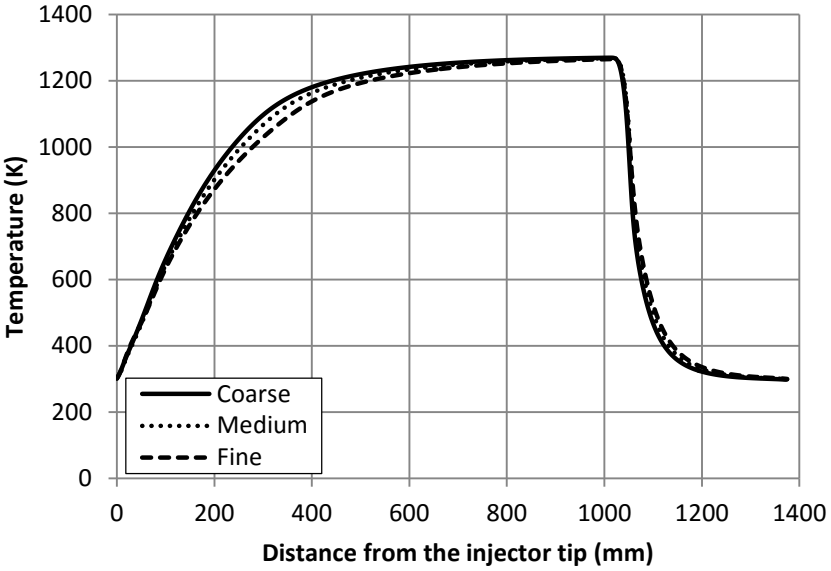

Figure 4.1 Temperature Distribution along the Centreline of the Reactor Obtained Using Three Different Meshes

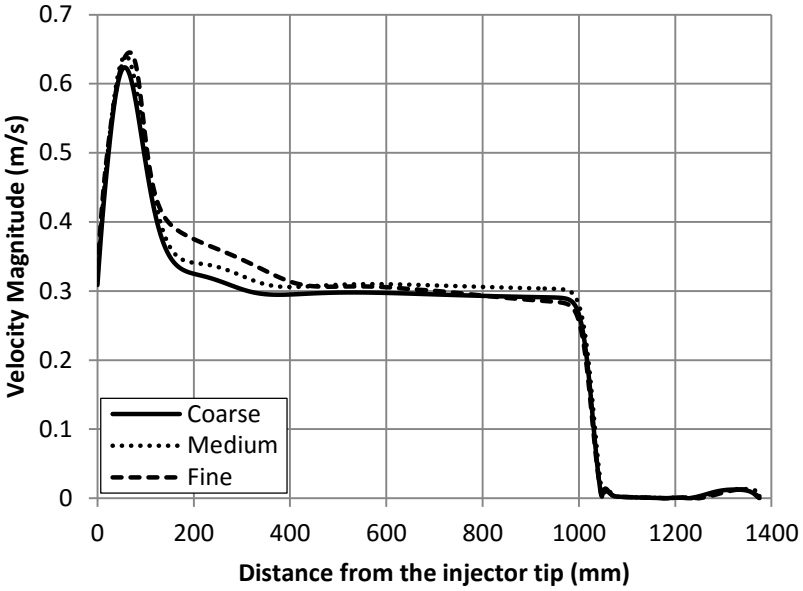

Figure 4.2 Velocity Magnitudes along the Centreline of the Reactor Obtained Using Three Different Meshes

4.2 Temperature Distribution inside the Drop Tube Furnace

In this section, temperature distribution results in the DTF obtained with three different turbulence models (Standard k-ε, Realizable k-ε, SST k-ω) are presented by using quarter DTF models. Steady solution is used for k-ε models. SST k-ω model is solved as transient to achieve convergence. Therefore, time-average temperature results for SST k-ω model are obtained in order to compare to steady solution. Then CFD results are compared with the experimental results. Temperature distribution results on a symmetry plane are demonstrated in Figure 4.3 and 4.4.

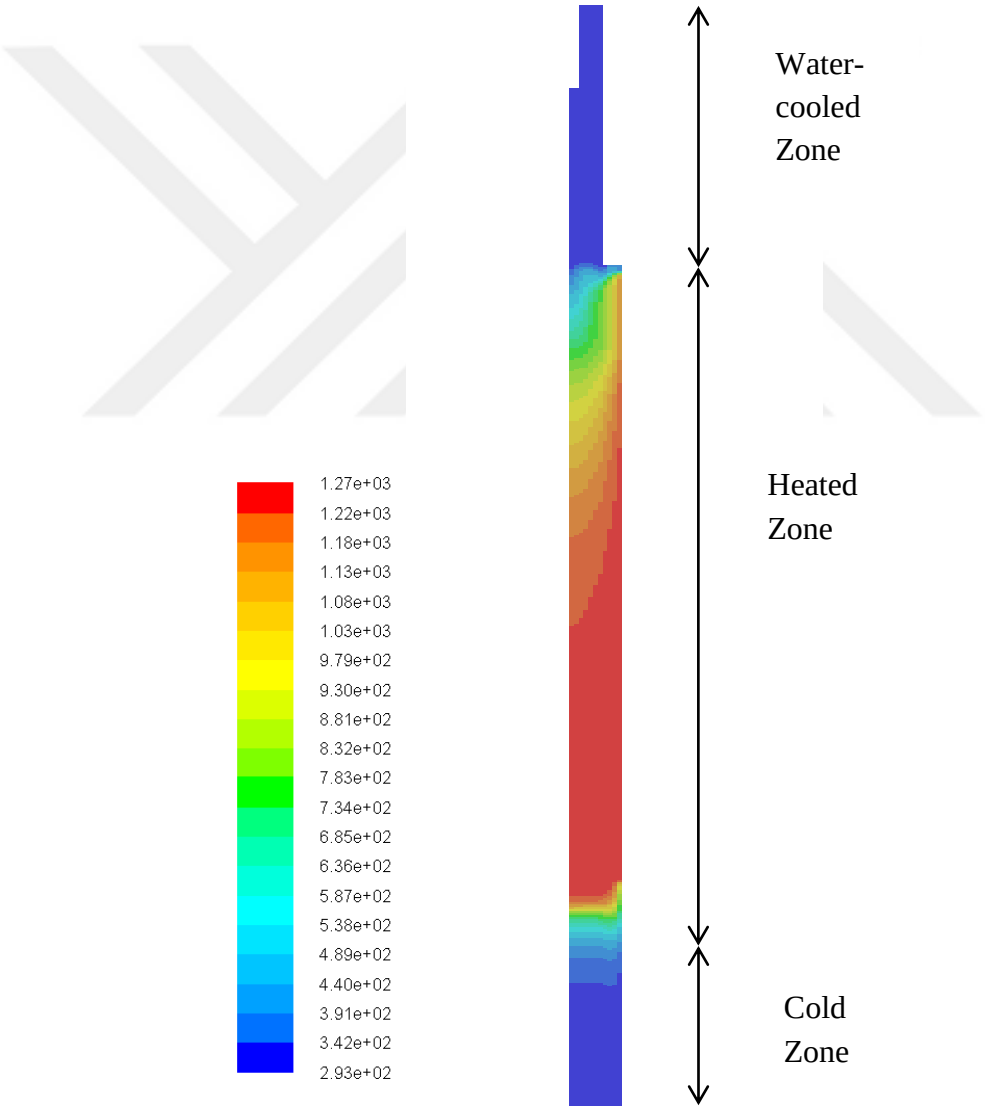

Figure 4.3 Temperature (K) Distribution inside the DTF (k-ε model)

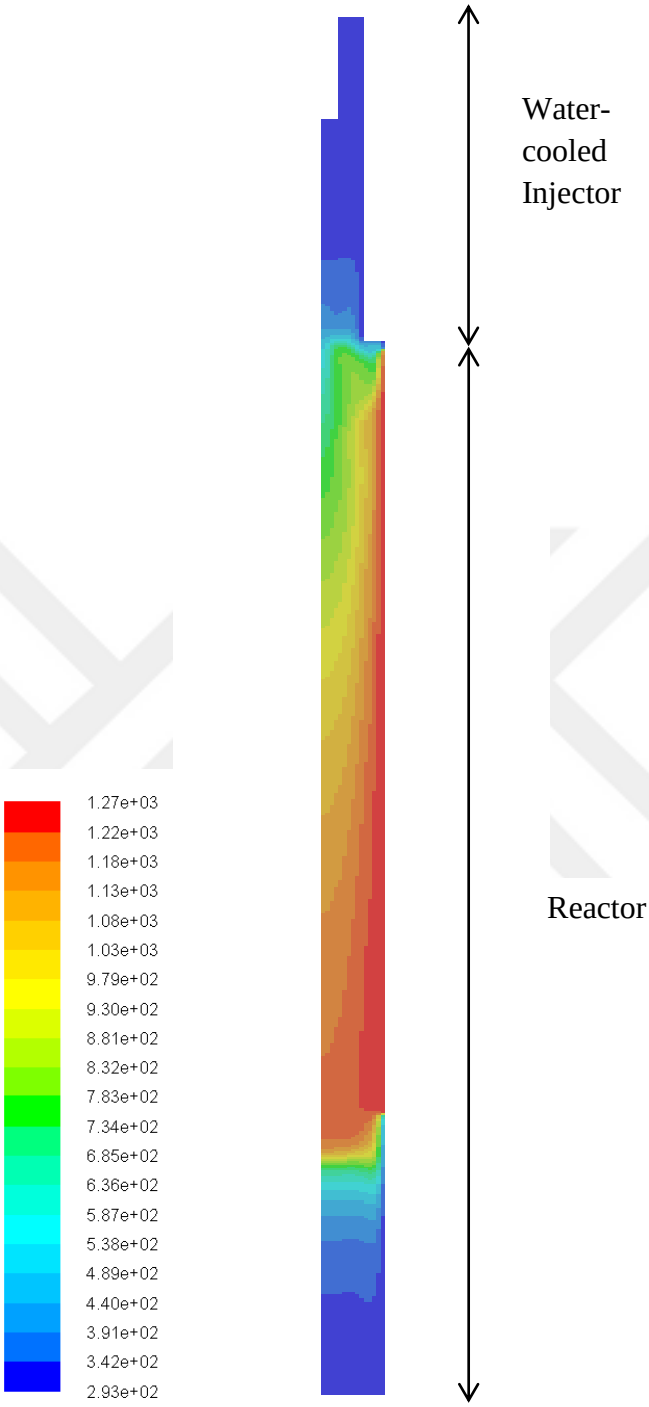

Figure 4.4 Mean Temperature (K) Distribution inside the DTF (k-ω model)

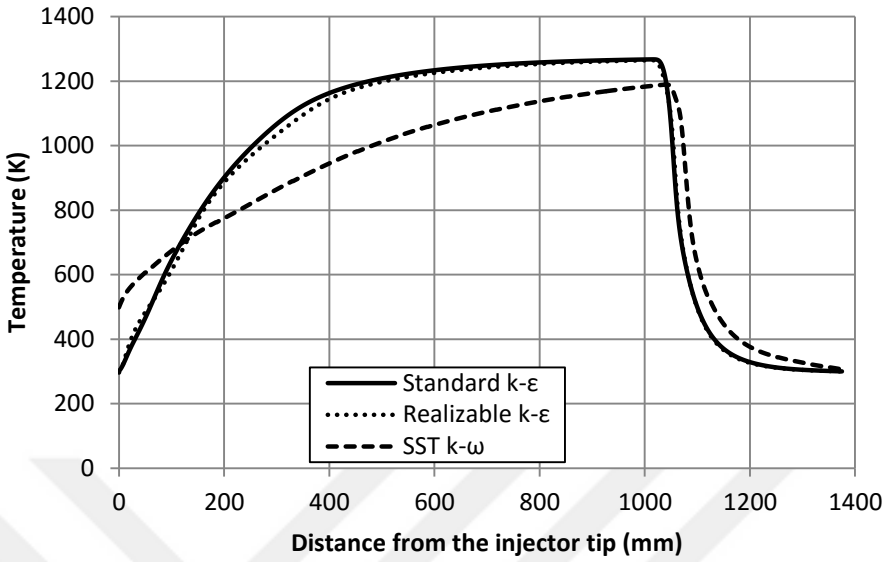

Figure 4.5 Temperature along the Centreline of the Reactor Obtained Using Three Different Turbulence Models

The temperature results along the centreline of the reactor obtained using three different turbulence models are demonstrated in Figure 4.5. As indicated in Figure 4.5, the temperature along the centreline of the reactor results obtained by using Standard and Realizable k-ε turbulence models are almost the same. Comparison of the results of the analysis performed using the SST k-ω model and those of the analysis performed using k-ε models shows that the results are more or less the same after 1000 mm distance from the tip point of the injector. However, until the mentioned point, lower temperature values are obtained with the SST k-ω model except at the entrance of the reactor, when compared to k-ε models. Analyses performed using k-ε models result with constant temperature zone. On the other hand, with the analysis performed using the k-ω model, no absolute constant temperature zone could be obtained. The aim of this study is to obtain constant temperature zone as in case of real boilers. k-ε models results provide that.

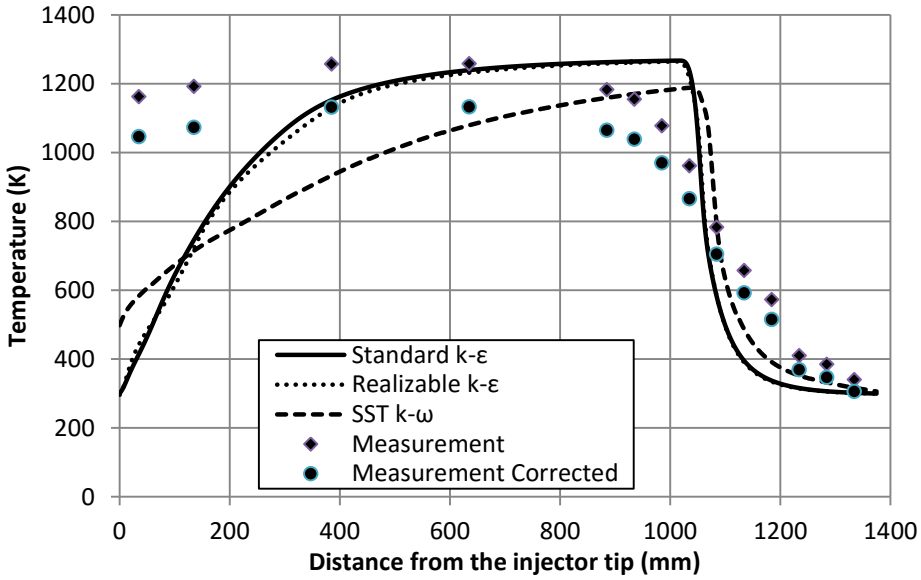

Figure 4.6 CFD and Experimental Results for Temperature along the Centreline of the Reactor

The results obtained with CFD simulations should be compared with experimental results for validation. Therefore, numerical and experimental results are compared in this study, as can be seen in Figure 4.6. Temperature measurements are presented under the graph, both as corrected and uncorrected values. Radiation correction of thermocouple measurement is introduced in the section of 3.2. Corrected measurement results are lower than the uncorrected measurement results, as a result of which analysis results, especially the temperature values obtained with the k-ε model, are higher than the corrected temperature values. This could be related to constant temperature boundary condition selection. Constant temperature boundary condition is applied for the wall surfaces, and convection and radiation are not calculated in the analyses separately. The largest difference between the analysis results and the measurements performed is at the reactor entry. This difference is due to either numerical or experimental reasons. Some simplifications (model, mesh, boundary conditions) are made for the CFD simulations performed in this thesis. These simplifications may be the reason for the errors. Constant temperature boundary condition is used for the water-cooled injector.

This selection can be one of the most important reasons for the difference between numerical and experimental results at the entrance of the reactor. Besides, the diameter of the bead of the thermocouple is large that creates uncertainity. On the other hand, reviewing the similar studies available under the literature, it can be seen that similar trends, as can be seen in Figures 2.1, 2.4, 2.5, are observed in experimental and numerical results. In literature, as can be seen in [37] and [41], the expertimental results are not presented at the entrance of the reactor. In studies [37], [41] and [42], there is a sharp rise in analysis results at the reactor entry. This condition shows that the prediction of the temperature values at the entrance of the reactor is difficult with CFD analysis. Results obtained with the k-ε model have more similar trends to both experimental and literature results, when compared to k-ω model. Also, with these results, the desired constant temperature zone could be obtained. Radial temperature results are also demonstrated in Figures 4.7. Reviewing the radial temperature results, it is understood that a constant temperature zone is formed 810 mm away from the tip of the injector in the analysis performed based on the k-ε model. On the other hand, in the analysis performed based on the k-ω model, there is approximately 100 K temperature difference between the centre point and the surface.

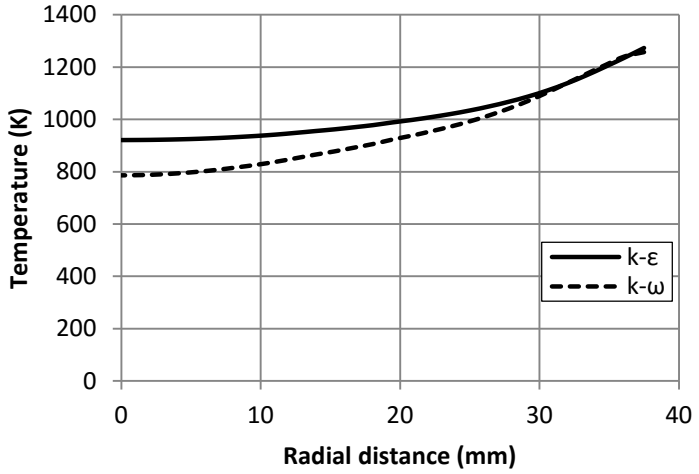

a)

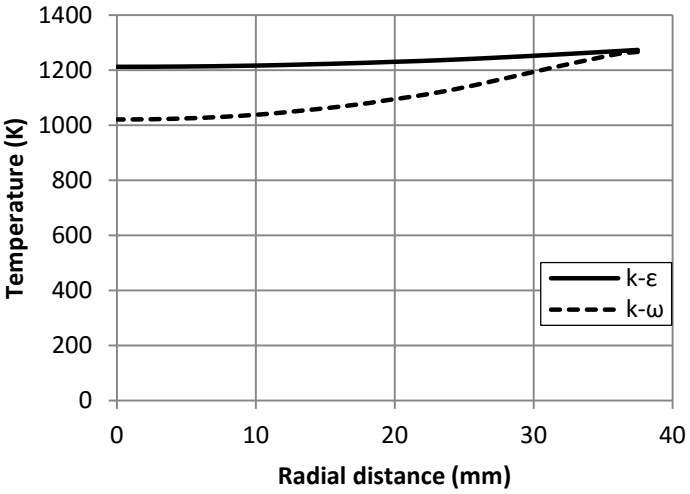

b)

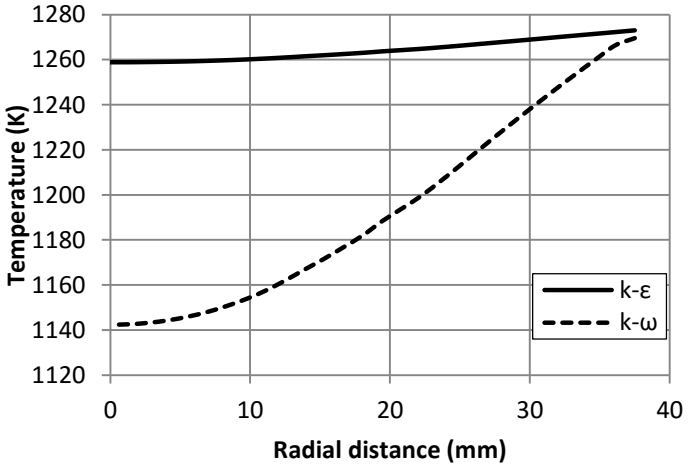

c)

Figure 4.7 Radial Temperature at a) 210 mm, b) 510 mm, c) 810 mm Distance from the Injector Tip

4.3 Velocity Magnitudes inside the Drop Tube Furnace

In this section, velocity magnitudes, as can be seen in Figure 4.8 and 4.10, are obtained with three different turbulence models (Standard k-ε, Realizable k-ε, SST k-ω). Mean velocity magnitudes are presented for SST k-ω model. The results are demonstrated on a symmetry plane.

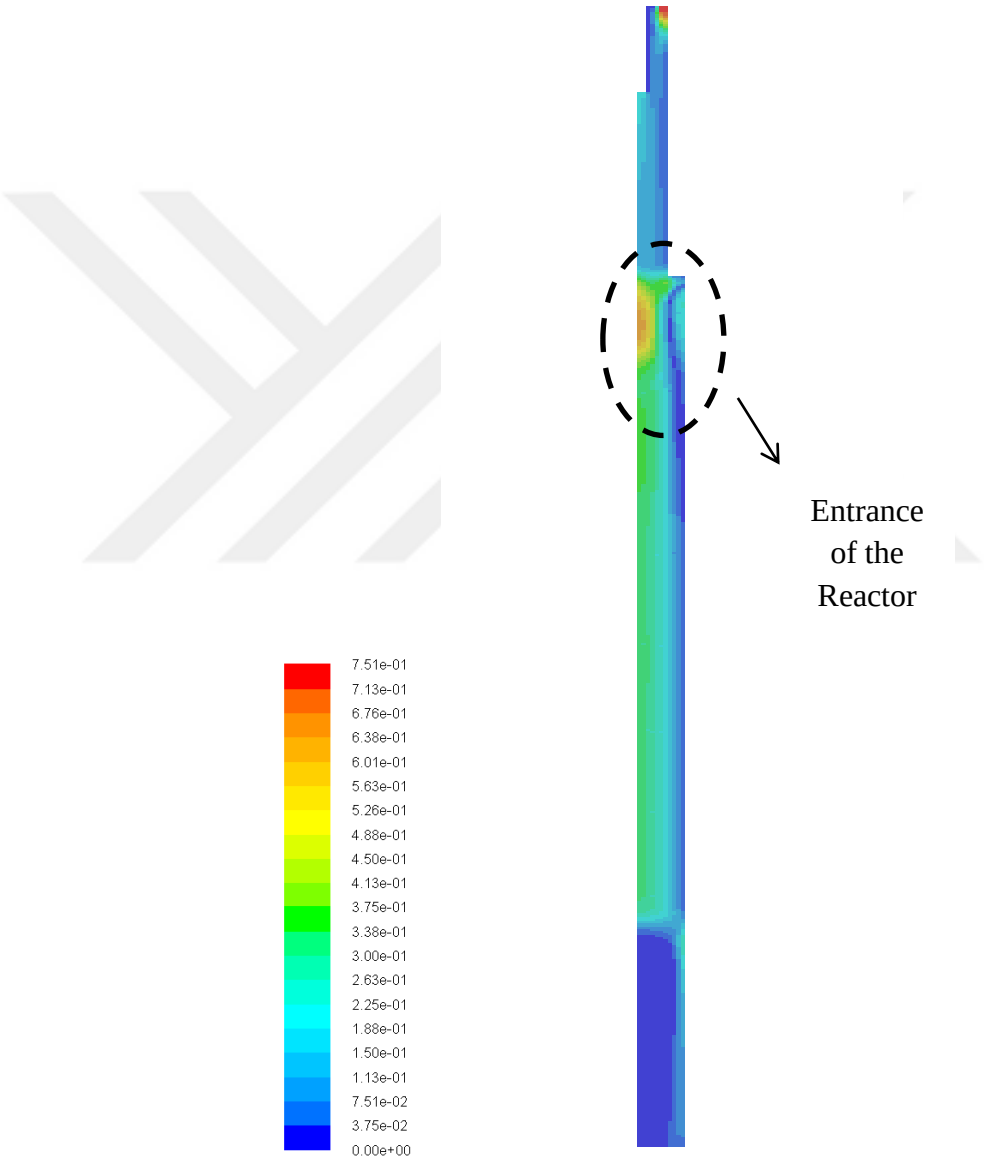

Figure 4.8 Velocity Magnitudes (m/s) in the DTF (k-ε model)

Moreover, the pathlines are created so that recirculation zones at the entrance of the reactor are observed, as can be seen in Figure 4.9. Recirculation zones are required and essential especially for combustors to stabilize the flame in the near burner region and ensure sufficient particle residence time to reach burnout.

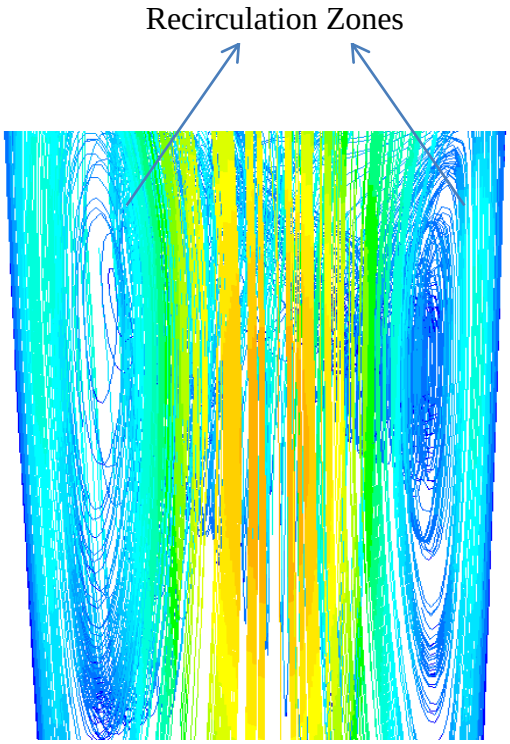

Figure 4.9 Recirculation Zones at the Entrance of the Reactor (k-ε model)

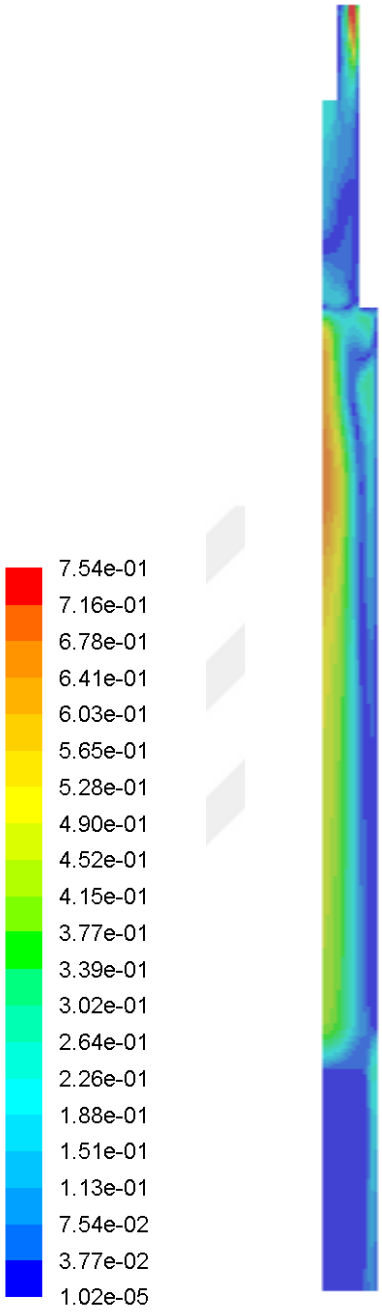

Figure 4.10 Mean Velocity Magnitudes (m/s) in the DTF (k-ω model)

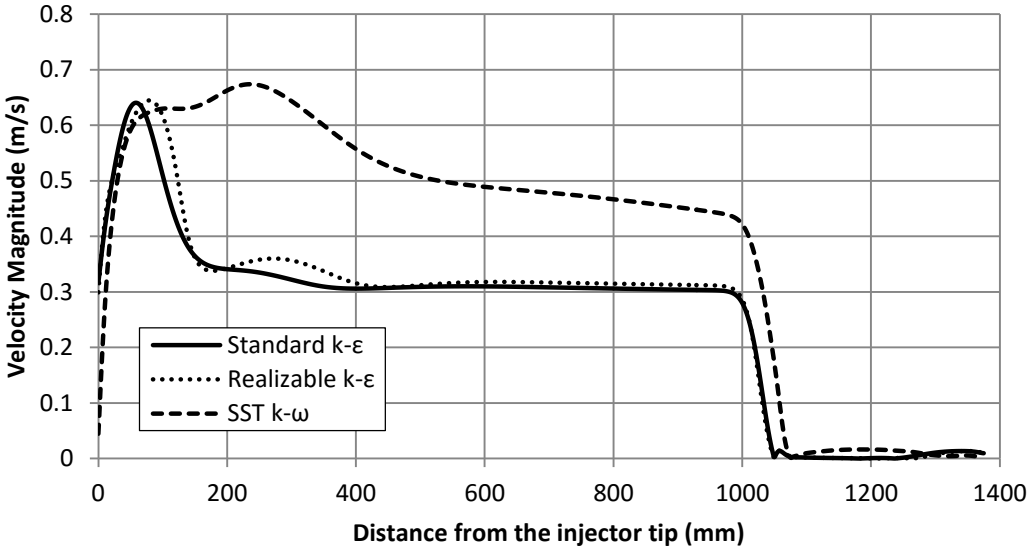

Figure 4.11 Velocity Magnitudes along the Centreline of the Reactor Obtained Using Three Different Turbulence Models

Velocity magnitudes along the centreline of the reactor obtained using three different turbulence models are presented in Figure 4.11. As shown in Figures 4.8, 4.10 and 4.11; with the results obtained with the SST k-ω model, it is observed that the velocity is higher along the centreline. In the analyses performed based on both models, k-ω and k-ε models, the flow rate accelerates at the entrance of the reactor, and then gets stable at a fixed rate after decreasing. Compared to the k-ω model, the analyses performed based on the k-ε models are resulted with more constant velocity zones. Velocity results in the literature also show that the air continues to flow with a constant velocity, as can be seen in Figures 2.4 and 2.5. Analyses performed on three models prove that the flow reaches a stagnation region within the cold zone. Hence, a vacuum pump is required to maintain the flow through the furnace. Information about the flow and approximately velocity magnitudes inside the DTF are obtained thanks to CFD simulations performed in this thesis. According to the analysis results, Reynolds number is calculated as 143 inside the constant temperature zone. Gr/Re^2 parameter is validated inside the heating zone based on this calculation. Gr/Re^2 is higher than 1. Consequently, natural convection governs the flow inside the heating zone.

4.4 Gravitational Effect on the Flow

Natural convection is the dominant phenomenon in the drop tube furnace according to the non-dimensional parameters. Natural convection occurs due to temperature differences in the domain with gravity. The analysis in which gravity is not taken into account is performed in order to investigate the effect of buoyancy forces on the flow. Standard k-ε model is employed for this investigation. Figure 4.12 and 4.13 demonstrate the results of the analysis in which gravity is neglected.

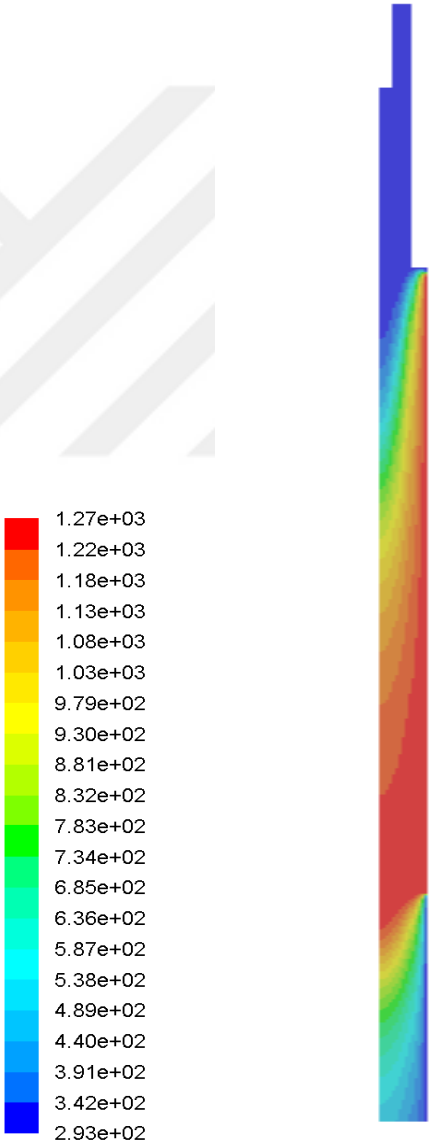

Figure 4.12 Temperature Distribution (K) in the DTF (Standard k-ε model – without gravity)

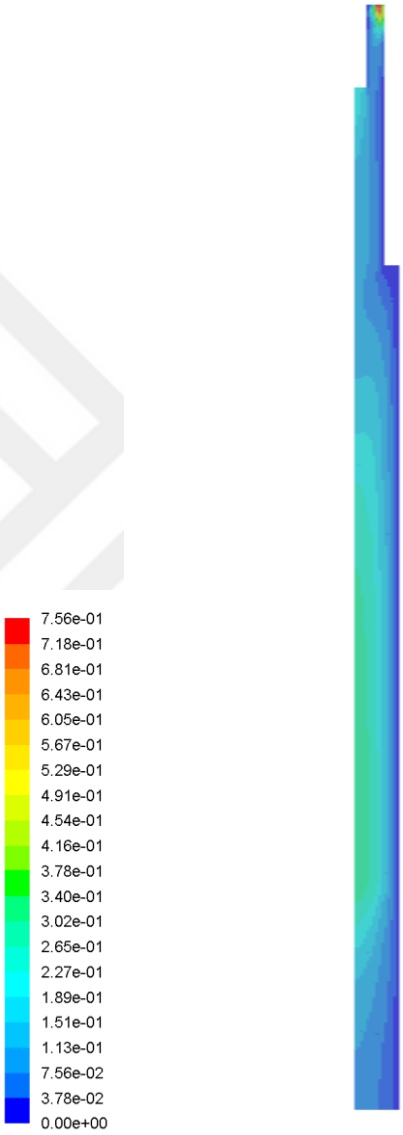

Figure 4.13 Velocity Magnitudes (m/s) in the DTF (Standard k-ε model – without gravity)

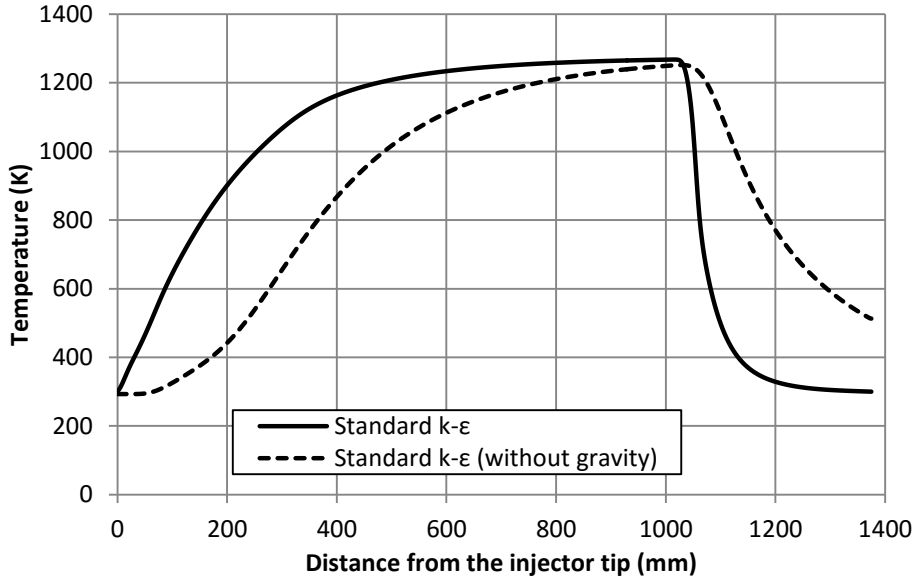

Figure 4.14 Gravitational Effect on Temperature Distribution along the Centreline of the Reactor

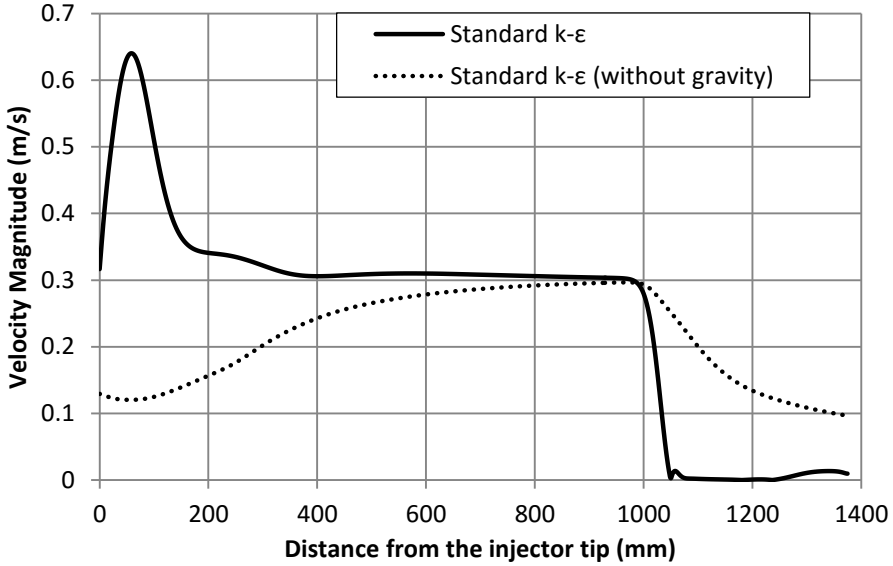

Figure 4.15 Gravitational Effect on Velocity Magnitudes along the Centreline of the Reactor

In the analyses with gravitational effect, the flow is stagnant at the cold zone. On the other hand, in the analysis where gravity is not taken into account, the air continues to flow within the whole reactor, as can be seen in Figure 4.15. In the analysis where gravity is not taken into account, the flow gets warmer more slowly in the heated zone, and the constant temperature zone cannot be obtained. Demonstrating these effects, how the buoyancy forces change the flow within the furnace is analysed.

CHAPTER 5

CONCLUSIONS

5.1 Summary and Conclusion

The flow inside the drop tube furnace, which is utilized for the experiments conducted within the scope of TÜBİTAK project is characterized with non-dimensional parameters and CFD simulations. Reynolds, Grashof, Prandtl, Rayleigh, and Nusselt numbers are calculated in order to determine the dominant phenomena and the type of the flow regime inside the DTF. Temperature distribution and velocity magnitudes inside the DTF are calculated with CFD simulations without taking the fuel combustion into account in this study. Total air volumetric rate entering the inlets is 10 lpm and the heated surface of the reactor is 1273 K for the experiments performed within the scope of TÜBİTAK project. Therefore, same boundary conditions are employed for the CFD simulations carried out in this thesis. A simplified quarter model is created for the CFD analysis of the DTF. Three different structured mesh constructions are generated to study mesh independence. Three different turbulence models (Standard k-ε, Realizable k-ε, SST k-ω) are used for the analyses in order to determine the suitable model for the study. Due to the fact that natural convection which occurs due to temperature differences in the domain with gravity effect is dominant phenomenon inside the DTF, gravitational effect on the flow is investigated. The following conclusions are obtained with this study.

- The non-dimensional parameters calculated in this study demonstrate that natural convection governs the flow inside the drop tube furnace, because Gr/Re^2 is higher than 1.

- In case of natural convection, Grashof number is also a crucial dimensionless number to decide the flow type except Reynolds number. Whereas the flow is turbulent at inlets based on the Reynolds number, turbulence is observed in the flow within the zone that is heated according to the Grashof number.
- Medium mesh is sufficient for the CFD analysis of the DTF among the mesh constructions generated in this thesis.
- Due to the fact that the flow is turbulent inside the DTF, three different turbulence models are utilized for the simulations to be able to calculate velocity magnitudes and temperature distribution. The results of the simulations performed with Standard and Realizable k-ε model are almost the same. These results provide more similar trends to both the results in literature and experimental results when compared to k-ω model. Moreover, isothermal zone is obtained with the simulations in which k-ε models are used.
- Recirculation zones are observed at the entrance of the reactor.
- Analysis results show that flow rate increases at the entrance of the reactor, and then gets stable with a decreasing.
- According to the results of the simulations, the flow is stagnant within the cold zone. Therefore, a vacuum pump is needed to maintain the flow through the furnace.
- Natural convection is the dominant phenomenon inside the DTF, which is why buoyancy forces influence on the flow is observed in the analyses performed. Unlike the natural convection analyses, the flow is not stagnant at a certain point, but continues to flow. Thereby, the velocity magnitude and temperature values are different from the results of the natural convection simulations.

5.2 Future Work

- Some simplifications (model, mesh, boundary conditions) are made for the purposes of this study. The accuracy of these simplifications can be evaluated by decreasing these simplifications and observing their impacts on the analysis results.
- The constant temperature is used as boundary condition in this thesis. This problem can be also solved as a conjugate heat transfer problem, thus the results obtained with two methods can be compared.
- With the analyses conducted using the Large Eddy Simulation (LES) model, more detailed information about the flow can be obtained; therefore, LES model can be utilized as a transient solution. On the other hand, LES model is not preferred within the scope of this thesis with the aim of decreasing the computational time.
- The analyses performed under this thesis study are for determining whether the furnace in the laboratory reflects the actual boiler conditions or not, and whether there is appropriate flow for the combustion or not. Thus, further studies can be performed by taking the fuel combustion into account. Considering the combustion analyses within the drop tube furnace under the literature and the results of this thesis study, k-ε model should be preferred for the combustion analysis.

REFERENCES

[1] P.J. Reddy, Clean Coal Technologies for Power Generation, CRC Press, 2014

[2] Key World Energy Istatistics 2017, http://www.iea.org, last visited on October 2017

[3] X. Jiang, D. Chen, Z. Ma and J. Yan, Models for the combustion of single solid fuel particles in fluidized beds: A review, Renewable and Sustainable Energy Reviews 68, pp. 410-431, 2017

[4] S. Sadaka and D.M. Johnson, Biomass Combustion, Agriculture and Natural Resources, University of Arkansas Division of Agriculture

[5] D.A. Tillman, Combustion Engineering Issues for Solid Fuel Systems, Introduction

[6] D.A. Tillman, The Combustion of Solid Fuels and Wastes, Academic Press, 1991

[7] https://www.worldcoal.org/coal/what-coal, last visited on September 2017

[8] X. Shen, Coal Combustion and Combustion Products, Coal, Oil Shale, Natural Bitumen, Heavy Oil and Peat- Vol. I

[9] Coal, Global Warming, and Health, Coal's Assault on Human Health, Physicians for Social Responsibility

[10]http://fluid.wme.pwr.wroc.pl/~spalanie/dydaktyka/combustion_MiBM/BCS/COAL_COMBUSTION.PDF, last visited on December 2016

[11] The Complete Book on Biomass Based Products (Biochemicals, Biofuels, Activated Carbon), NIIR Board of Consultants & Engineers, Asia Pacific Business Press Inc., 2015

[12] Study on Biomass Combustion Emissions, Irish Bioenergy Association, 2016

[13] H. Tolvanen, T. Keipi and R. Raiko, A study on raw, torrefied, and steam-exploded wood: Fine grinding, drop-tube reactor combustion tests in N2/O2 and CO2/O2 atmospheres, particle geometry analysis, and numerical kinetics modeling, Fuel 176, pp. 153-164, 2016

[14] P. McNamee, L.I. Darvell, J.M. Jones and A. Williams, The combustion characteristics of high-heating-rate chars from untreated and torrefied biomass fuels, Biomass and Bioenergy 82, pp. 63-72, 2015

[15] indianpowersector.com/home/power-station/thermal-power-plant, last visited on July 2017

[16] www.energy.kth.se/compedu/webcompedu/manualcopy, last visited on July 2017

[17] www.brighthubengineering.com/power-plants/differences, last visited on August 2017

[18] J. Blondeau, Investigation of pulverised biomass combustion: detailed modelling of particle pyrolysis and experimental analysis of ash deposition, Ecole Polytechnique de Louvain, Thesis, 2013

[19] M. Cloke, E. Lester and A.W. Thompson, Combustion characteristics of coals using a drop tube furnace, Fuel 81, pp. 727-735, 2002

[20] J. B. A. Card and A. R. Jones, A Drop Tube Furnace Study of Coal Combustion and Unburned Carbon Content Using Optical Techniques, Combustion and Flame 101, pp. 539 547, 1995

[21] M. R. Avila, M. Honkanen, R. Raiko and A. Oksanen, Coal char combustion in O2/N2 and O2/CO2 conditions in a drop tube reactor: an optical study, Industrial Combustion, 2012

[22] G. Wang, R. Zander and M. Costa, Oxy-fuel combustion characteristics of pulverized-coal in a drop tube furnace, Fuel 115, pp. 452-460, 2014

[23] L. Chen, S. Z. Yong and A. F. Ghoniem, Oxy-fuel combustion of pulverized coal: Characterization, fundamentals, stabilization and CFD modeling, Progress in Energy and Combustion Science 38, pp. 156-214, 2012

[24] E. Rokni and Y. A. Levendis, Utilization of a High-Alkali Lignite Coal Ash for SO2 Capture in Power Generation, J. Energy Eng., ASCE, 2016

[25] S. Zellagui, G. Trouve, C. Schönnenbeck, N. Zouaoui-Mahzoul and J.F. Brilhac, Parametric study on the particulate matter emissions during solid fuel combustion in a drop tube furnace, Fuel 189, pp. 358-368, 2017

[26] T. Chi, H. Zhang, Y. Yan, H. Zhou and H. Zheng, Investigations into the ignition behaviors of pulverized coals and coal blends in a drop tube furnace using flame monitoring techniques, Fuel 89, pp. 743-751, 2010

[27] L. Cai, C. Zou, Y. Guan, H. Jia, L. Zhang and C. Zheng, Effect of steam on ignition of pulverized coal particles in oxy-fuel combustion in a drop tube furnace, Fuel 182, pp. 958-966, 2016

[28] F.F. Costa, G. Wang and M. Costa, Combustion kinetics and particle fragmentation of raw and torrefied pine shells and olive stones in a drop tube furnace, Proceedings of the Combustion Institute 35, pp. 3591-3599, 2015

[29] Ndibe, J. Maier and G. Scheffknecht, Combustion, cofiring and emissions characteristics of torrefied biomass in a drop tube reactor, Biomass and Bioenergy 79, pp. 105-115, 2015

[30] V. Branco and M. Costa, Effect of particle size on the burnout and emissions of particulate matter from the combustion of pulverized agricultural residues in a drop tube furnace, Energy Conversion and Management, 2017

[31] S. Zellagui, T. Decaix, C. Schönnenbeck, G. Leyssens, O. Allgaier, N. Zouaoui-Mahzoul, E. Thunin, O. Authier, P. Plion, L. Porcheron and J.F. Brilhac, Pyrolysis of coal and woody biomass under N_2 and CO_2 atmospheres using a drop tube furnace, International Flame Research Foundation, 2015

[32] G. Wang, R.B. Silva, J.L.T. Azevedo, S. Martins-Dias and M. Costa, Evaluation of the combustion behaviour and ash characteristics of biomass waste derived fuels, pine and coal in a drop tube furnace, Fuel 117, pp. 809-824, 2014

[33] Y. Wang, X. Wang, Z. Hu, Y. Li, S. Deng, B. Niu and H. Tan, NO Emissions and combustion efficiency during biomass co-firing and air-staging, Bioresources, 2015

[34] S. P. Visona and B. R. Stanmore, Modeling Nitric Oxide Formation in a Drop Tube Furnace Burning Pulverized Coal, Combustion and Flame 118, pp. 61-75, 1999

[35] C. Schönenbeck, R. Gadiou and D. Schwartz, A kinetic study of the high temperature NO–char reaction, Fuel 83, pp. 443–450, 2004

[36] J.M. Jones, M. Pourkashanian, A. Williams and D. Hainsworth, A comprehensive biomass combustion model, Renewable Energy 19, pp. 229-234, 2000

[37] B. Feron, Numerical and experimental characterization of a drop tube furnace and ash deposition analysis, Ecole Polytechnique de Louvain, Master Thesis, 2013

[38] J. Zhang, W. Prationo, L. Zhang and Z. Zhang, CFD Modelling of the oxy-fuel combustion of Victorian Brown Coal in Drop Tube Furnace and 3MW Pilot Scale Boiler, Ninth International Conference on CFD in the Minerals and Process Industries, 2012

[39] E.I. Jassim, CFD Modeling of Toxic Elements evolved during Coal Combustion, Proceedings of The Canadian Society for Mechanical Engineering International Congress, 2014

[40] J. Hart, A. H. Al-Abbas and J. Naser, Numerical investigation of pyrolysis of a Loy Yang coal in a lab-scale furnace at elevated pressures, Heat Mass Transfer 49, pp. 1725–1732, 2013

[41] G. Wang, (Co-) combustion of solid fuels: experiments and modeling, Universidade de Lisboa, PhD Thesis, 2014

[42] D. Fan, Y. Mohassab, M. Elzohiery and H.Y. Sohn, Analysis of the Hydrogen Reduction Rate of Magnetite Concentrate Particles in a Drop Tube Reactor Through CFD Modeling, The Minerals, Metals & Materials Society and ASM International, 2016

[43] Radiation correction of thermocouples, www.matfys.lth.se/education/FMFF05, last visited on September 2017

[44] www.thermalfluidscentral.org, last visited on September 2017

[45] J.P. Holman, Heat Transfer, McGraw-Hill Series in Mechanical Engineering, 10th Edition, 2009

[46] V.V. Ranade and D.F. Gupta, Computational Modeling of Pulverized Coal Boilers, CRC Press, 2014

[47] FLUENT User's Guide

[48] H. Schlichting, Boundary Layer Theory, 7th Edition, McGraw Hill Book Company, 1979

[49] ITU Ninova, ninova.itu.edu.tr/tr/dersler/ucak-uzay.../ekkaynaklar?, last visited on May 2017

APPENDIX A

AN EXAMPLE OF RADIATION CORRECTION CALCULATION

The required equations for the calculation are given in (A.1) and (A.2). Parameters and values which are used in radiation correction calculation are presented in Table A.1 for 1200 K. 1200 K is given as an example for temperature measured by thermocouple.Radiation correction calculation is carried out with the parameters in Table A.1 by using (A.1) and (A.2).

$$\Delta T = T_g - T_{TC} = (\varepsilon \sigma T_{TC}^4)/h \tag{A.1}$$

$$h = (\frac{k_c}{d})(2 + 0.6\left(\frac{c_p \mu}{k}\right)^{0.33} (\frac{Vd\rho}{\mu})^{0.5} \tag{A.2}$$

Table A.1 Parameters for the Radiation Correction Calculation

Parameters	Values
ϵ	0.35
σ	$5.67*10^{-8}$ W/m^{2}K^4
T_{TC}	1200 K
k_c	0.0782 W/m.K
d	0.5 mm
C_p	1.179 kJ/kg.K
μ	$4.69*10^5$ kg/m.s
V	0.3 m/s
ρ	0.2947 kg/m^3

APPENDIX B

THE PROPERTIES OF AIR

Incompressible Ideal Gas Law, FLUENT

$$\rho = \frac{P_{op}}{\frac{R}{M_w}T} \tag{B.1}$$

R= the universal gas constant

M_w= Molecular weight

P_{op}= Operating pressure

Specific Heat Capacity, Polynomial

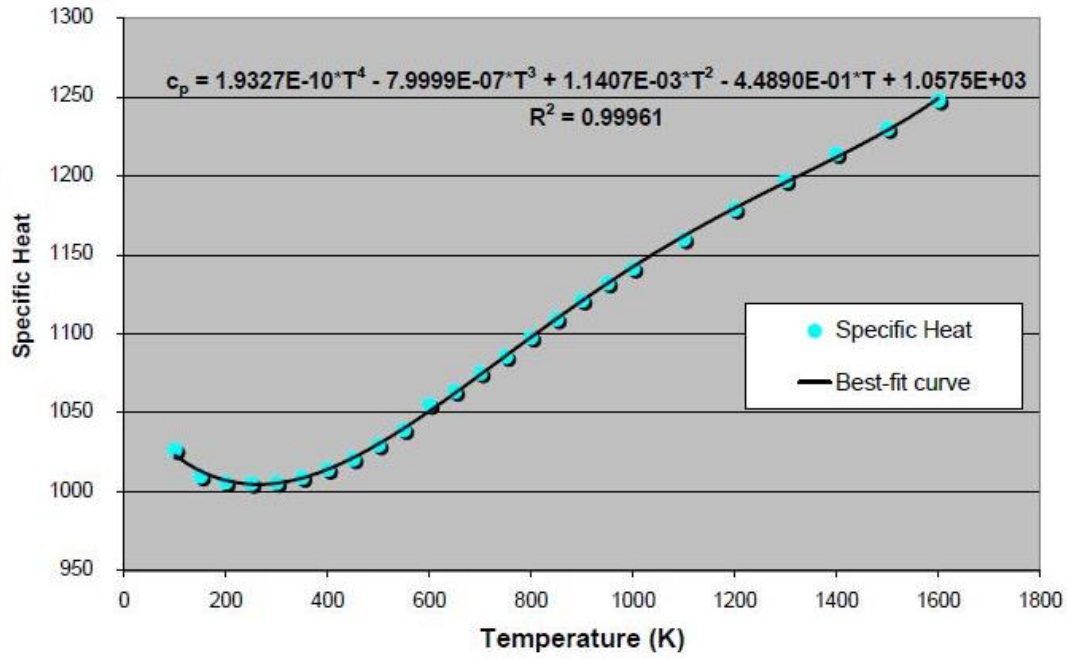

Figure B.1 Specific Heat Capacity – Temperature [49]

Thermal Conductivity, Polynomial

EXCEL GRAPH

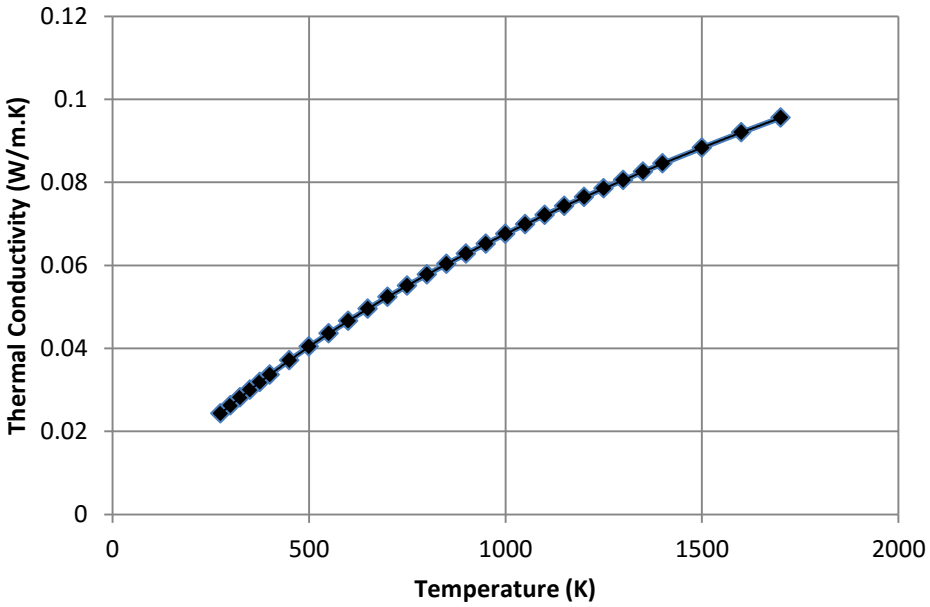

Figure B.2 Thermal conductivity – Temperature

Polynomial function is $y=-4e\text{-}15T^4+2e\text{-}11T^3-5e\text{-}08T^2+0.0001T-0.0006$ for thermal conductivity of air.

Viscosity of air

Sutherland Law with three coefficients, FLUENT

$$\mu = \mu_0 (\frac{T}{T_0})^{3/2} \frac{T_0+S}{T+S} \quad \text{(B.2)}$$

μ= viscosity kg/m.s

μ_0= reference value

T= static temperature K

T_0= an effective temperature (Sutherland constant)